Summer 8-2022

Foundations for Finite-State Modelling of a Two-Dimensional Airfoil that Reverses Direction

Jake Michael Oscar Welsh

WASHINGTON UNIVERSITY IN ST. LOUIS

McKelvey School of Engineering
Department of Mechanical Engineering & Materials Science

Thesis Examination Committee:
David Peters, Chair
Mark Jakiela
Swami Karunamoorthy

Foundations for Finite-State Modelling of a Two-Dimensional Airfoil that Reverses Direction

by
Jake Michael Oscar Welsh

A thesis presented to
the McKelvey School of Engineering
of Washington University
in partial fulfillment of the
requirements for the degree
of Master of Science

August 2022
St. Louis, Missouri

Table of Contents

List of Figures

List of Symbols

b	=	Airfoil Half-Chord Length
b_n	=	Binomial Expansion Coefficients
C_l	=	Lift Coefficient
D	=	Nondimensional Distance
f	=	Reverse Flow Factor
G	=	Mirrored Total Bound Vorticity
h	=	Plunge Distance
k	=	Nondimensional Frequency
k_n	=	Mirrored Glauert Coefficients for Induced Flow Due to Shed Vorticity
L	=	Lift
n	=	Indicial State Number
N	=	Total Number of States
r	=	Distance from Velocity Measurement Point to Infinitesimal Vorticity in Wake
s	=	Nondimensional Distance Between Airfoil and Vorticity Segment
t	=	Time
T	=	Nondimensional Distance a Fluid Particle Will Travel
u_0	=	Free-stream Velocity
v	=	Induced Velocity Due to Bound Vorticity
v_0	=	Average Free-Stream Velocity
w_n	=	Glauert Coefficients for Flow Due to Airfoil Motion
x	=	Coordinate System

α	=	Angle of Attack
Γ	=	Total Bound Vorticity
γ_b	=	Bound Vorticity on the Airfoil
Δ	=	Distance Airfoil is Engulfed by Phantom Vorticity Segment
ϵ	=	Small Nondimensional Distance Used in Cauchy Integration
θ	=	Glauert Induced Flow Coordinate System
λ	=	Induced Velocity Due to Shed Vorticity
λ_n	=	Glauert Coefficients for Induced Flow Due to Shed Vorticity
λ_0	=	Average Induced Flow Over Airfoil
μ	=	Amplitude
μ_0	=	Mirrored Frees-tream Velocity
ξ	=	Transformed Coordinate System
ρ	=	Free-stream Density
τ	=	Nondimensional Time
ϕ	=	Glauert Variable
ω_n	=	Mirrored Glauert Coefficients for Flow Due to Airfoil Motion

Acknowledgements

I would like to thank Dr. David A Peters for guidance, assistance, and inspiration throughout the duration of the research presented here.

I would like to thank Drs. Timothy Jackson, Emily Boyd, and Vladimir Kurenok for their instruction and aid during my time at Washington University.

I would like to thank Dr. Henry Pernicka of Missouri University of Science and Technology for instilling in me an interest to pursue graduate work and a passion for flight mechanics.

This research was partially funded through the U.S. Army/Navy/NASA Vertical Lift Research Center of Excellence at Georgia Tech under the direction of Mahendra Bhagwat of the US Army Futures Comment, Agreement No. W911W6-21-2-0001. Opinions, interpretations, conclusions, and recommendations are those of the authors and are not necessarily endorsed by the United States Government.

Jake M.O. Welsh

Washington University in St. Louis

August 2022

Dedicated to My Parents.

ABSTRACT OF THE THESIS

Foundations for Finite-State Modelling of

a Two-Dimensional Airfoil that Reverses Direction

by

Jake Michael Oscar Welsh

Master of Science in Aerospace Engineering

Washington University in St. Louis, 2022

Professor David Peters, Chair

Current 3-D finite-state wake models are incapable of simulating a maneuver in which the sign of the free-stream velocity changes direction and the rotor enters its own wake – as might occur in the case of a helicopter which ascends and then descends. It is the purpose of this work to create a 2-D finite-state wake model which is capable of handling changes in free-stream direction as a precursor to development of a 3-D model that can do the same.

The 2-D finite-state model used for reentry modifications is an existing model created by Peters, Johnson, and Karunamoorthy. By the addition of a parameter which changes the sign of the free-stream accordingly, a model capable of handling forward and backward flight is developed and tested.

Upon testing of the model for an oscillatory free-stream which changes direction, it was discovered that the presence of a singularity causes the system to become unstable. This behavior was determined to be due to a Floquet instability which occurs in periodic free-streams that reverse direction.

Several analytical expressions for the motion of a segment of vorticity in the wake are developed and presented as test cases for future work on an oscillatory free-stream. The finite-state model is found to accurately approximate the effect of the wake vorticity on the airfoil airloads, paving the way for future investigations when the airfoil changes directions and enters its own wake.

Chapter 1:

Introduction

1.1 Previous Work

Three papers form the foundation for the work presented here. The most influential being *Finite-State Airloads Modeling with Compressibility and Unsteady Free-Stream* by Peters and Barwey. The paper compares the results of finding the effect of free-stream oscillations and compressibility on the lift of thin airfoils in two dimensions using a finite-state model to those of Isaacs and the Arbitrary Motion Theory.

Peters and Barwey's paper combines elements from two other papers, *Finite-State Airloads for Deformable Airfoils on Fixed and Rotating Wings*, by David Peters and Mark Johnson, and *State-Space Inflow Models for Rotor Aeroelasticity*, by David Peters and Swaminathan Karunamoorthy. Modifications to the concepts presented in these three papers are the subject of the research presented here.

1.2 Motivation for Extending Model

The finite-state model described in Peters and Barwey does not incorporate the effects of reverse flow upon the lift generation. Reverse flow is when the flow impinges upon the trailing edge of the airfoil, as happens over part of the rotor blade in forward flight. The original theory by Peters and Johnson includes the effect of reversed flow on the Kutta condition but not on the induced flow due to shed vortices.

The goal of including reverse flow into the 2-D model is to eventually extend the model

to 3-D such that it will be capable of simulating what happens when a vehicle (most likely a helicopter or similar vehicle) were to change direction and fly back into its own wake. Whether that be vertically such as take-off and landing in its own wake, or horizontally by flying forwards and then changing directions and flying backwards. Being able to compute the physics of performing such a maneuver in a flight simulator will increase the overall accuracy of the simulation, improving flight training programs or saving time and funds during design analysis.

1.3 Current Approach

Beginning from the model presented in Barwey, a mirror-image approach was taken to generate a model capable of handling reverse flow. By flipping the direction of the airfoil and the freestream, and performing a change of variables, a finite-state model which could operate in reverse flow was developed. The results of this new model showed a singularity which would occur when the flow would change direction.

Several processes were implemented to determine the source of the singularity, which resulted in the determination that the instability was a Floquet instability caused by energy being transferred into the system by the flow changing direction.

1.4 Closed-Form Benchmarks

The next goal was to replace the bound vorticity, Γ, developed by an airfoil dependent on angle of attack with that of a specified Γ. In this way a user of the model can input whatever bound vorticity is created by any object in flight and thus make the code more viable for general use. The finite-state model was re-derived to implement such a scenario but needed a closed-form model to compare results with.

A closed-form equation describing a smooth segment of vorticity developed by some arbitrary shape in flight was chosen to compare results with due to its simplified form. Expressions of the segment's vorticity were developed to describe what would happen as a segment is generated at the trailing edge of the airfoil, and then what would happen as the complete segment would move further away and eventually return to the airfoil.

Chapter 2:

Fluid Mechanics of Basic Equations

There are three texts which form the basis for the research presented in the following chapters. The first is Ref. [1], *Finite-State Airloads for Deformable Airfoils on Fixed and Rotating Wings*, by David Peters and Mark Johnson. The second is Ref. [3], *State-Space Inflow Models for Rotor Aeroelasticity*, by David Peters and Swaminathan Karunamoorthy. The final is Ref. [2], *Finite-State Airloads Modeling with Compressibility and Unsteady Free-Stream*, by David Peters, Dinesh Barwey, and Mark Johnson. For ease of reference, these three papers will be refferred to as the Johnson, Swami, and Barwey papers respectively.

2.1 Johnson's Airloads

Johnson's paper presents a state-space method for the development of lift and drag on a deformable airfoil in both two and three dimensions. Johnson describes an airfoil placed in a 2-D coordinate system with an airfoil placed on the x-axis such that $-b < x < b$. The flow velocities in the x and y-directions are described by u_0 and v_0 respectively. He then describes the airfoil in terms of the Glauert Variable ϕ, which allows him to convert the airloads equations into ordinary differential equations via Glauert Expansion. The airfoil coordinate system is shown below, and is subsequently used in the analysis presented in Chapter 3 and Chapter 4 with the exception that the airfoil never leaves the x-axis so the value of $h(x,t)$ is zero.

Johnson's derivation is highly descriptive throughout the process, and results in a general airloads model which he then converts to matrix form to solve for an expression for the lift and pitching moment using state-space methods. However, an issue with Johnson's model is

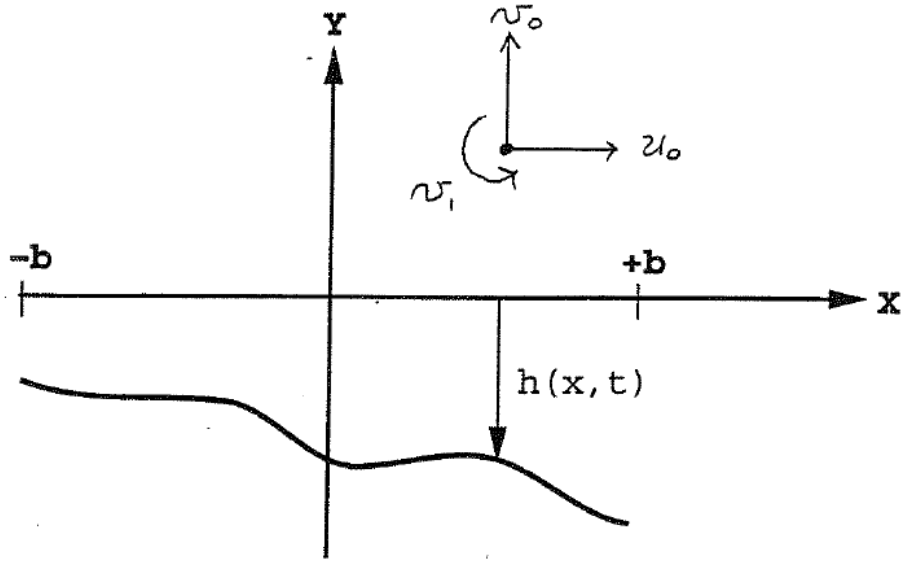

Figure 2.1: General Airfoil Coordinate System (Taken Directly from Ref. [1])

that an expression for λ_0 (which is a forcing function) was not provided, and the user would have to provide their own expression for it via their own means. Swami's paper remedies this.

2.2 Swami's Coefficients

Swami's paper outlines the development of a state-space inflow model using 2-D thin airfoil theory. He then extends the model to a case where the bound circulation is changed by the effects of dynamic stall.

Like Johsnon, Swami uses a state-space representation of the induced velocity coefficients, λ_n to describe the airloads on the airfoil. However, Swami also developed an expression for λ_0 in terms of the λ_n and binomial expansion coefficients, b_n:

$$\lambda_0 = \frac{1}{2}\sum_{n=1}^{N} b_n \lambda_n \tag{2.1}$$

This allows the model to solve for the value of λ_0 without needing the expression given to

it via other means. Swami's results matched those of Theodorsen and Wagner using this method.

2.3 Barwey's Unification

Barwey's paper set out to combine and apply a unified version of Johnson and Swami's papers. Barwey takes the airloads equations for Johnson and uses them in conjunction with Swami's equation for λ_0. Barwey subsequently tests the effects of an airfoil placed in a periodic free-stream and compares his model to existing data from Isaacs and Greenberg, finding that the finite-state model accurately approximates the results of both. The results of the airloads from this paper are provided in the Appendix.

The results presented for the oscillatory flow in Barwey form the starting point for the research presented in the following chapters. It is desired to create an extension of Barwey's finite-state model such that the model is capable of handling flows which move in reverse. Testing the finite-state model against the results of Barwey's oscillatory flow provides experimental data with which to validate the reverse flow version.

Chapter 3:

Extensions From Mirror-Image Approach

3.1 The Original Peters-Barwey Model

It is important to first understand the finite-state inflow theory in its mathematical form. In Peters and Barwey a derivation of a nondimensional state space model for determining the Glauert induced flow coefficients, λ_n, shown below.

$$[A]\{\bar{\lambda}_n\}^* + \bar{u}_0(t)\{\bar{\lambda}_n\} = \{c\}(\bar{w}_0 + \bar{w}_1/2)^* \tag{3.1}$$

Eqn. (3.1), when coupled with the equations below, where [A] and {c} are defined later in this chapter, provides a full description of the loads upon a thin airfoil.

$$\bar{L}_c = \bar{u}_0(\bar{w}_0 + \frac{1}{2}\bar{w}_1 - \bar{\lambda}_0) \tag{3.2}$$

$$\bar{\lambda}_0 = \frac{1}{2}\sum_{n=1}^{N} b_n \bar{\lambda}_n \tag{3.3}$$

$$\bar{C}_{lc} = (\bar{w}_0 + \frac{1}{2}\bar{w}_1 - \bar{\lambda}_0)/\bar{u}_0 \tag{3.4}$$

Eqn. (3.1) is the nondimensional matrix form of the differential equations for induced flow.

The inflow in index form is given by:

$$b(\dot{\lambda}_0 - \frac{1}{2}\dot{\lambda}_2) + u_0\lambda_1 = \dot{\Gamma}/\pi \tag{3.5}$$

$$\frac{b}{2n}(\dot{\lambda}_{n-1} - \dot{\lambda}_{n+1}) + u_0\lambda_n = \dot{\Gamma}/(n\pi) \quad n \geq 2 \tag{3.6}$$

$$\Gamma = 2\pi b(w_0 + \frac{1}{2}w_1 - \lambda_0 - \frac{1}{2}\lambda_1) \tag{3.7}$$

Where the b_n coefficients used in Eqn. (3.3) are defined by:

$$b_n = (-1)^{n+1}\frac{(N+n+1)!}{(N-n-1)!}\frac{1}{(n!)^2} \quad n \neq N \tag{3.8}$$

$$b_N = (-1)^{N+1} \tag{3.9}$$

It is important to note the definitions: $\bar{w}_0^* = \bar{u}_0^*\alpha + \bar{u}_0\dot{\alpha} + \ddot{h} - a\ddot{\alpha}$, $\bar{w}_1^* = \ddot{\alpha}$, and $\bar{u}_0 = 1 + \mu sin(k\tau)$. Velocities ($u_0$, λ_n, w_n) have been nondimensionalized on the average free-stream velocity (v_0). Lift has been normalized on $L_0 = 2\pi\rho b v_0^2$. Time is nondimensionalized such that $\tau = v_0 t/b$ and $(\ )^*$ is the derivative with respect to τ. In order to transform differential equations Eqn. (3.5) and (3.6) into the finite-state model (Eqn. (3.1)), the differntial equations must be nondimensionalized.

Peters and Barwey test three cases of α: $\alpha = 1$, $\alpha = sin(k\tau)$, and $\alpha = cos(k\tau)$, and determine the lift and lift coefficients developed by each case after all transients have decayed from the system.

Expanding out the [A] and {c} matrices created from Eq. (3.1), it can be seen that the matrices follow a set pattern for any number of states N.

$$A = \begin{bmatrix} \frac{3}{2}b_1 + 1 & \frac{3}{2}b_2 - \frac{1}{2} & \frac{3}{2}b_3 & \frac{3}{2}b_4 & \frac{3}{2}b_5 & \frac{3}{2}b_6 & \dots \\ \frac{1}{2}b_1 + \frac{3}{4} & \frac{1}{2}b_2 & \frac{1}{2}b_3 - \frac{1}{4} & \frac{1}{2}b_4 & \frac{1}{2}b_5 & \frac{1}{2}b_6 & \dots \\ \frac{1}{3}b_1 + \frac{1}{3} & \frac{1}{3}b_2 + \frac{1}{6} & \frac{1}{3}b_3 & \frac{1}{3}b_4 - \frac{1}{6} & \frac{1}{3}b_5 & \frac{1}{3}b_6 & \dots \\ \frac{1}{4}b_1 + \frac{1}{4} & \frac{1}{4}b_2 & \frac{1}{4}b_3 + \frac{1}{8} & \frac{1}{4}b_4 & \frac{1}{4}b_5 - \frac{1}{8} & \frac{1}{4}b_6 & \dots \\ \frac{1}{5}b_1 + \frac{1}{5} & \frac{1}{5}b_2 & \frac{1}{5}b_3 & \frac{1}{5}b_4 + \frac{1}{10} & \frac{1}{5}b_5 & \frac{1}{5}b_6 - \frac{1}{10} & \dots \\ \frac{1}{6}b_1 + \frac{1}{6} & \frac{1}{6}b_2 & \frac{1}{6}b_3 & \frac{1}{6}b_4 & \frac{1}{6}b_5 + \frac{1}{12} & \frac{1}{6}b_6 & \dots \\ \vdots & \vdots & \vdots & \vdots & \vdots & \vdots & \ddots \end{bmatrix} \quad c = \begin{bmatrix} 2 \\ 1 \\ \frac{2}{3} \\ \frac{1}{2} \\ \frac{2}{5} \\ \frac{1}{3} \\ \vdots \end{bmatrix} \tag{3.10}$$

3.1.1 Validation of the MATLAB Model

The first step in the project was to take the theory described above and recreate it using MATLAB. Using the [A] and {c} matrices from before and $N = 8$ states, first a case of $\alpha = 1 - e^{-\tau}$ with $u_0 = 1$ and $\mu = 0$ was tested in a numerical ode solver (`ode45`) to determine the model's validity. The results of the lift and lift coefficient are shown below. A factor of $\alpha = 1 - e^{-\tau}$ was chosen as the test condition for the ODE solver due to its simplicity as well as its asymptotic nature. It can be seen that the values for lift and lift coefficient approach 1, as was expected, thus verifying that the time-step simulator was correct.

Next, the three cases of $\alpha = 1$, $\alpha = sin(k\tau)$, and $\alpha = cos(k\tau)$ were tested. In all three of these cases, $\mu = 0.8$ and $k = 0.2$. The results of which are shown below.

After running the simulator for all three cases, it was found that results exactly match the graphs provided in Barwey for the same μ and k. The Greenberg conditions of the same α values were also tested, and the graphs produced also match the Greenberg graphs provided in Barwey, further proving the MATLAB model's validity. These can be found in the Appendix along with Barwey's original results.

The Peters and Barwey paper creates a concise and direct method for developing the

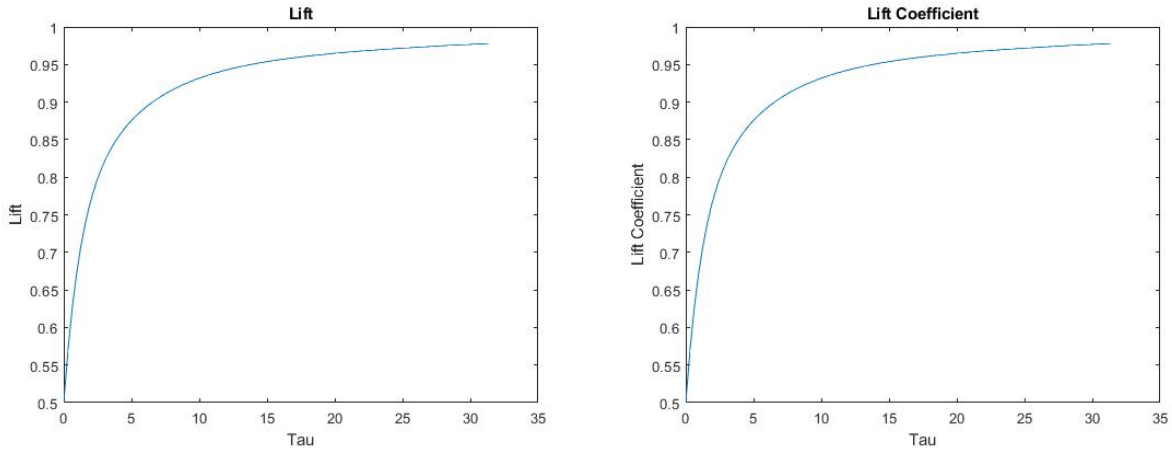

Figure 3.1: Lift and Lift Coefficient of $\alpha = 1 - e^{-\tau}$

loads on an airfoil, but fails to include reverse flow due to the shed vortices into its analysis. In the paper by Johnson and Peters, a similar state space method is developed, however including a factor f for the inclusion of reverse flow. In the next section, a description of implementing this factor from Johnson into the method developed in the Barwey paper is provided.

3.2 The Reverse Flow Model

To derive the equations used for reverse flow, the same principles used to derive the original state space model in both Barwey and Johnson were applied, however with the direction of the flow moving in the negative x direction.

The process was to first set up a mirror image (over the y-axis) of the flow impinging on the airfoil and then use the Johnson and Barwey equations to write those in the same form as the existing theory. Then, by comparison of the original and mirror-image variables, it was possible to write a change of variable to transform the mirror-image system into the original system. Comparing those equations with the original equations, it is important to note that some terms are of the same sign and some are of opposite sign. The opposite terms

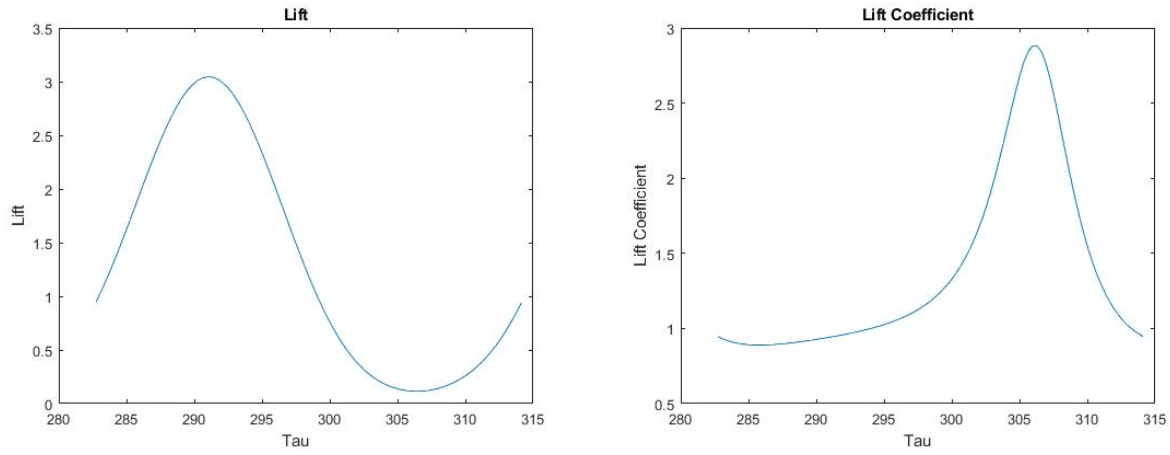

Figure 3.2: Lift and Lift Coefficient of $\alpha = 1$

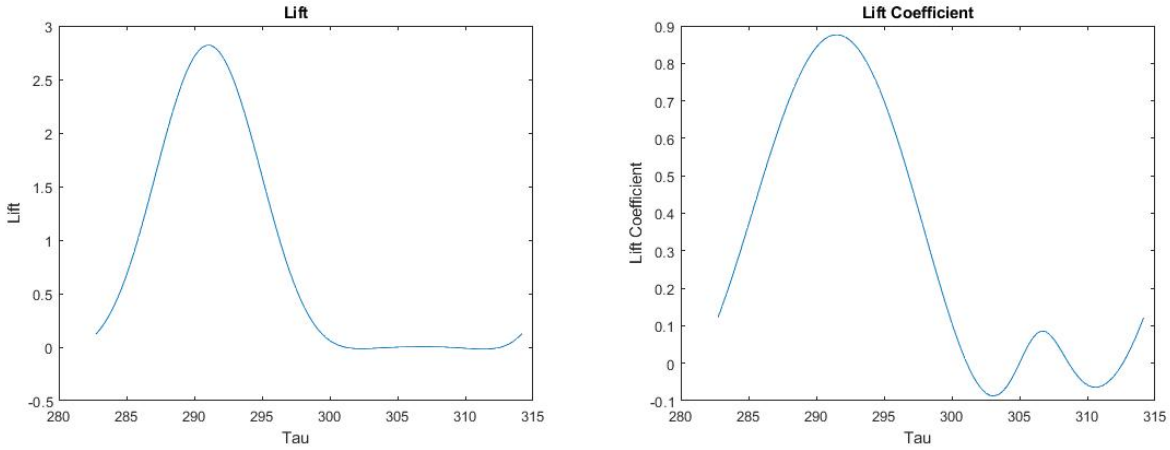

Figure 3.3: Lift and Lift Coefficient of $\alpha = sin(k\tau)$

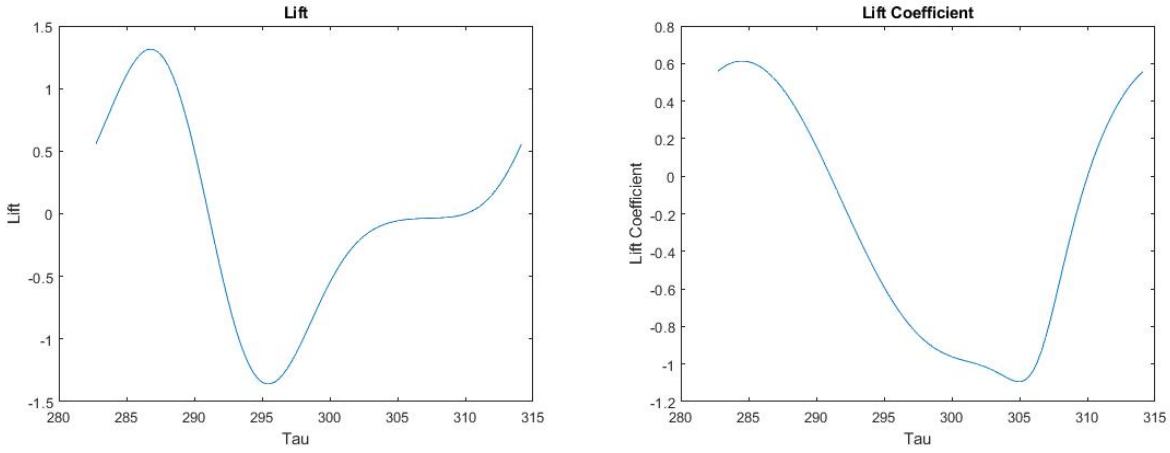

Figure 3.4: Lift and Lift Coefficient of $\alpha = cos(k\tau)$

are the ones that need to be changed for reversed flow. Thus, they are given the reverse-flow parameter f so that they will work in either regime. When flow is forwards, $f = 1$, when flow is backwards, $f = -1$. The mathematical conversion process is described below:

$$G = 2\pi b(\omega_0 + \frac{1}{2}\omega_1 - k_0 - \frac{1}{2}k_1) \tag{3.11}$$

$$b(\dot{k}_0 - \frac{1}{2}\dot{k}_2) + \mu_0 k_1 = \dot{G}/\pi \tag{3.12}$$

$$\frac{b}{2n}(\dot{k}_{n-1} - \dot{k}_{n+1}) + \mu_0 k_n = \dot{G}/(n\pi) \quad n \geq 2 \tag{3.13}$$

$$k_0 = \frac{1}{2}\sum_{n=1}^{N} b_n k_n \tag{3.14}$$

In order to return to the original forward flow domain, the following change of variables is applied:

$$\begin{aligned} G &= -\Gamma \\ \mu_0 &= -u_0 \\ \omega_n &= (-1)^n w_n \\ k_n &= (-1)^n \lambda_n \end{aligned}$$

Following the change of variables, Eqns. (3.11) – (3.14) transform into:

$$\Gamma = 2\pi b(-w_0 + \lambda_0 + \frac{1}{2}w_1 - \frac{1}{2}\lambda_1) \tag{3.15}$$

$$b(\dot{\lambda}_0 - \frac{1}{2}\dot{\lambda}_2) + u_0\lambda_1 = -\dot{\Gamma}/\pi \tag{3.16}$$

$$\frac{b}{2n}(\dot{\lambda}_{n-1} - \dot{\lambda}_{n+1}) + u_0\lambda_n = (-1)^n\,\dot{\Gamma}/(n\pi) \quad n \geq 2 \tag{3.17}$$

$$\lambda_0 = \frac{1}{2}\sum_{n=1}^{N}(-1)^n\, b_n\lambda_n \tag{3.18}$$

Finally, replacing the -1's with the factor for reverse flow, f, the following final system of equations is achieved.

$$\Gamma = 2\pi b[f(w_0 - \lambda_0) + \frac{1}{2}(w_1 - \lambda_1)] \tag{3.19}$$

$$b(\dot{\lambda}_0 - \frac{1}{2}\dot{\lambda}_2) + u_0\lambda_1 = f\ \dot{\Gamma}/\pi \tag{3.20}$$

$$\frac{b}{2n}(\dot{\lambda}_{n-1} - \dot{\lambda}_{n+1}) + u_0\lambda_n = \begin{cases} \dot{\Gamma}/(n\pi) & n = \text{even} \\ f\ \dot{\Gamma}/(n\pi) & n = \text{odd} \end{cases} \qquad n \geq 2 \tag{3.21}$$

$$\lambda_0 = \frac{1}{2}\sum_{n=1,3,5,7\ldots}^{N} f\ b_n\lambda_n + \frac{1}{2}\sum_{n=2,4,6,8\ldots}^{N} b_n\lambda_n \tag{3.22}$$

With the final equations developed, a new set of matrices for [A] and {c} is derived by converting Eqns. (3.19) – (3.22) into a nondimensional state space matrix form similar to that of Eqn. (3.1), shown here:

$$[A]\{\bar{\lambda}_n\}^* + \bar{u}_0(t)\{\bar{\lambda}_n\} = \{c\}(f\bar{w}_0 + \bar{w}_1/2)^* \tag{3.23}$$

The new [A] and {c} matrices follow the same pattern and have the same element values as the matrices developed in the original Barwey Model from Eqn. (3.10). However, the new matrices have an overlay of f factors multiplied element-wise to each of the element values.

The overlay of both matrices is shown below:

$$A = \begin{bmatrix} f & . & f & . & f & . & \dots \\ . & f & . & f & . & f & \dots \\ f & . & f & . & f & . & \dots \\ . & f & . & f & . & f & \dots \\ f & . & f & . & f & . & \dots \\ . & f & . & f & . & f & \dots \\ \vdots & \vdots & \vdots & \vdots & \vdots & \vdots & \ddots \end{bmatrix} \quad c = \begin{bmatrix} f \\ . \\ f \\ . \\ f \\ . \\ \vdots \end{bmatrix} \tag{3.24}$$

In this way, when the free-stream is moving forwards ($u_0 > 0$), the matrices are identical to the ones developed before. However when the free-stream is moving backwards ($u_0 < 0$), all the elements with an f overlayed will have their values multiplied by -1.

3.2.1 Validation of the Reverse Flow Model

Full Forward Flow

To test the validity of the new state-space model, Eqn. (3.23), the model was run with the original forward flow conditions to ensure that the new model worked in the forward regime. In this case, $u_0 = 1 + \mu sin(k\tau)$ and $f = 1$. There are four cases of angle of attack which were tested with $\alpha = 1 - e^{-\tau}$, $\alpha = 1$, $\alpha = sin(k\tau)$, and $\alpha = cos(k\tau)$. These conditions should be identical to Eq. (3.1) since $f = 1$. The results of which confirmed this as they exactly matched the results shown in Figs. 3.1 – 3.4.

Full Reverse Flow

Once the new state-space model was verified to work in the forward flow regime, it was time to test it in the reverse regime. No data for reverse flow exists to compare to, so to

overcome this the model was tested with opposite conditions as the original forward flow model. The original model uses positive inflow with a positive airfoil angle of attack, so by implementing a negative inflow with a negative angle of attack, the airfoil will "see" the same inflow conditions as the original forward flow conditions. The results of these conditions should exactly match the original results.

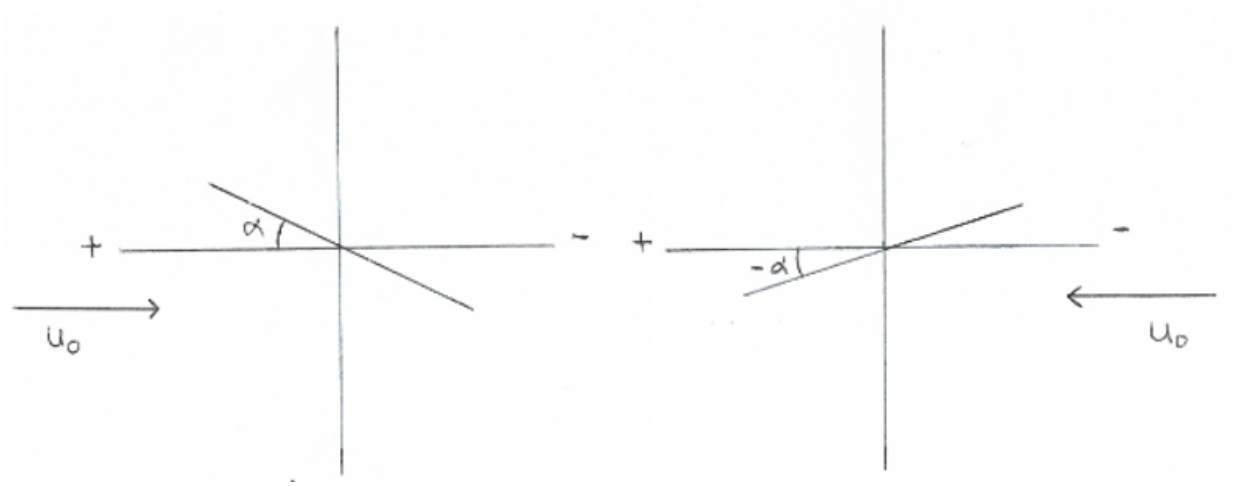

Figure 3.5: Original (Left) and Mirrored (Right) Flow Systems

To invert the free-stream conditions, a free-stream of $u_0 = -1 - \mu sin(k\tau)$ and a reverse flow factor of $f = -1$ was used. To reverse the airfoil motion, the four test conditions became $\alpha = -1 + e^{-\tau}$, $\alpha = -1$, $\alpha = -sin(k\tau)$, and $\alpha = -cos(k\tau)$. The results of these conditions exactly reproduced the results of Barwey (Figs. 3.1 – 3.4) just as the forward case had. As such it can be stated that the reverse flow model was valid for simulating flows with negative free-streams.

Transitional Flow

With a verification of the new reverse flow state-space model completed, it was time to develop a model capable of transitioning between forwards and reverse flow. Up until this point $\mu < 1$, and as such the inflow of $u_0 = 1 + \mu sin(k\tau)$ or $u_0 = -1 - \mu sin(k\tau)$ always

remained completely forwards or backwards, respectively. The transitional flow simulation will analyze the results of cases in which $\mu \geq 1$, which simulates oscillatory inflows that change direction during the course of the simulation. From this point on, $u_0 = 1 + \mu sin(k\tau)$ always.

To implement transitional flow into the simulation, the MATLAB `sign()` function was used on f. The line `f = sign(u0)` will cause MATLAB to assign $f = 1$ when u_0 is positive, $f = 0$ when u_0 is 0, and $f = -1$ when u_0 is negative. First the simulation was tested with $\mu < 1$ to ensure the `sign()` function was working correctly, then the case of $\mu \geq 1$ was examined. It became immediately apparent that that the ode45 solver was running into a singularity problem when f switched from positive to negative causing the code to "blow up" and time march to values of infinity. This can be seen in the figure below:

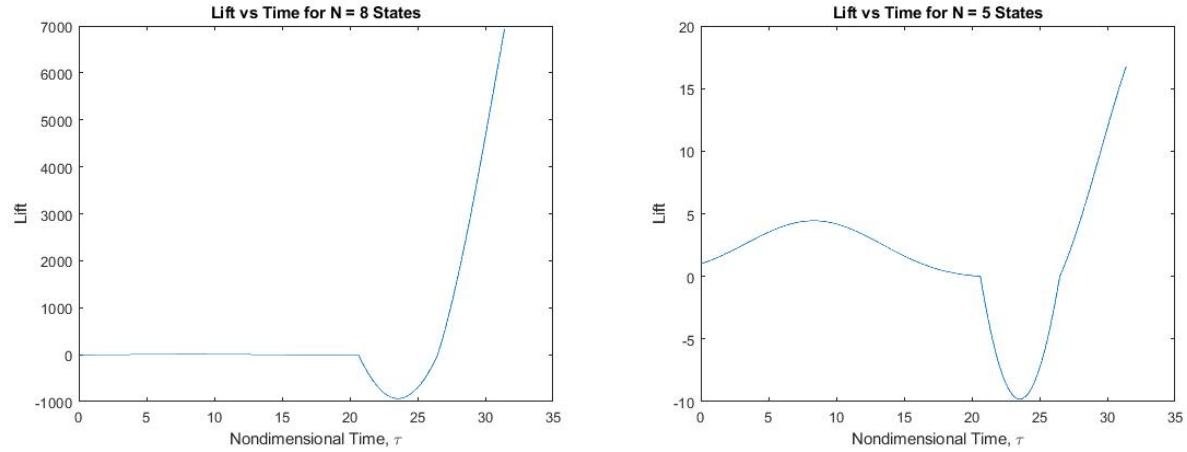

Figure 3.6: Transitional Flow Lift Response for $N = 5$ & $N = 8$

3.3 Numerical Issues and Attempts to Mitigate Them

Upon further inspection of the singularity, it was discovered that when extending the time-span over multiple periods, the singularity only produced unstable results for cases of $N \geq 5$.

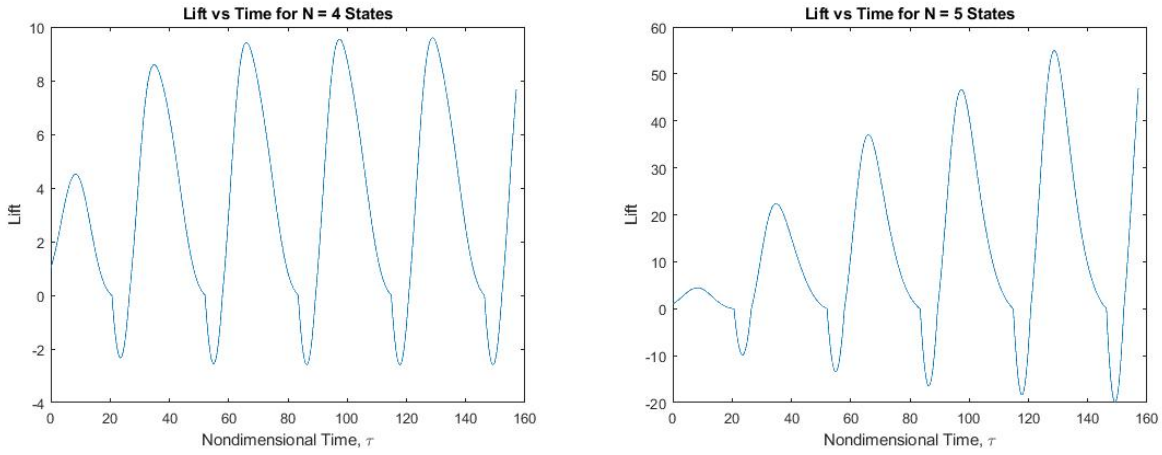

Figure 3.7: Singularity Lift Response Over 4 Periods

3.3.1 A More Robust Model

Initially, it was feared that the new state-space model was not robust enough to handle the switch from forward to reverse flow, and as such a more robust model was developed. Eqn. (3.23) was multiplied through by f algebraically resulting in the following equation:

$$[A]'\{\bar{\lambda}_n\}^* + f\bar{u}_0(t)\{\bar{\lambda}_n\} = \{c\}'(f\bar{w}_0 + \bar{w}_1/2)^* \tag{3.25}$$

In this new configuration of Eqn. (3.25), the robustness comes from the fact that the $\{\bar{\lambda}_n\}$ vector is never negative. Multiplying both [A] and {c} by f does not change the values of the elements in the matrices, but it does cause all of the terms that already had an f term to now include an f^2 term. All f^2 terms become 1, since f can only be 1 or -1, and both values squared produce 1. This changes the overlay of the f terms to now become:

$$A' = \begin{bmatrix} . & f & . & f & . & f & \dots \\ f & . & f & . & f & . & \dots \\ . & f & . & f & . & f & \dots \\ f & . & f & . & f & . & \dots \\ . & f & . & f & . & f & \dots \\ f & . & f & . & f & . & \dots \\ \vdots & \vdots & \vdots & \vdots & \vdots & \vdots & \ddots \end{bmatrix} \quad c' = \begin{bmatrix} . \\ f \\ . \\ f \\ . \\ f \\ \vdots \end{bmatrix} \tag{3.26}$$

To verify this new robust model, three cases of f were examined, as well as four cases of α and u_0. In the MATLAB script, f is determined by user input and can be one of three options: `f = 1` (only forwards), `f = -1` (only reverse), and `f = sign(u0)` (transitional) to accommodate all possible cases of f. As a sanity check, four cases were run with the full reverse flow option to ensure that the robust model was achieving correct results. These cases are as follows:

$$\alpha = 1, u_0 = 1 + \mu sin(k\tau)$$

$$\alpha = -1, u_0 = -1 - \mu sin(k\tau)$$

$$\alpha = 1, u_0 = -1 - \mu sin(k\tau)$$

$$\alpha = -1, u_0 = 1 + \mu sin(k\tau)$$

In this "sanity check," $\mu = 0.8$ and $k = 0.2$ which are the same conditions outlined in the Barwey paper, allowing results to be compared to the known correct ones. The results of this sanity check can be found in Figs. 5 – 8 in the Appendix. It is noted that the first and second cases exactly reproduce the results of the old model which were proven to match Barwey. The third and fourth cases are reflected versions of the original model which was expected. The results of all four of these cases validate the robust model.

When the robust model was run with $\mu \geq 1$, it again yielded the results shown in Fig. 3.6 in which a singularity occurred when the flow transitioned from forwards to reverse. Similar to Fig. 3.7, the robust model was capable of solving the linear system without becoming unstable for the case of $N < 5$. From this point on during the model's analysis, the robust model from Eq. (3.25) was used to synthesize results. While the robust model did not solve the singularity issue, it did prove that the singularity was not caused by a switching of $\{\lambda_n\}$ values from positive to negative.

3.3.2 Soft Reverse Flow

Due to the sharp nature of the kink in the graphs at the singularity's occurrence, it was hypothesized that the ode45 solver was having difficulty fitting a fourth-order curve through a non-differentiable point. Several theories about the nature of the numerical error were conceived, the first of which considered that perhaps the sharp instantaneous jump in the reverse flow factor from positive to negative 1 was causing issues for the solver.

To combat this, a "soft" reverse flow factor was developed:.

$$f = \frac{\bar{u}_0}{\sqrt{\bar{u}_0 + 0.01\lambda_0^2}} \tag{3.27}$$

The soft reverse flow equation creates a continuous curve through the step function for f when f is close to 0, eliminating the discontinuity that occurs during the switch from forward to reverse flow, shown below. Testing this however, did not result in any improvement to the singularity, ruling out the f factor as a source of error.

3.3.3 The Stop-Start Method

The next method tested was to stop and start the solver before and after the singularity. Since it was known that the model was capable of finding the correct solution in the forward

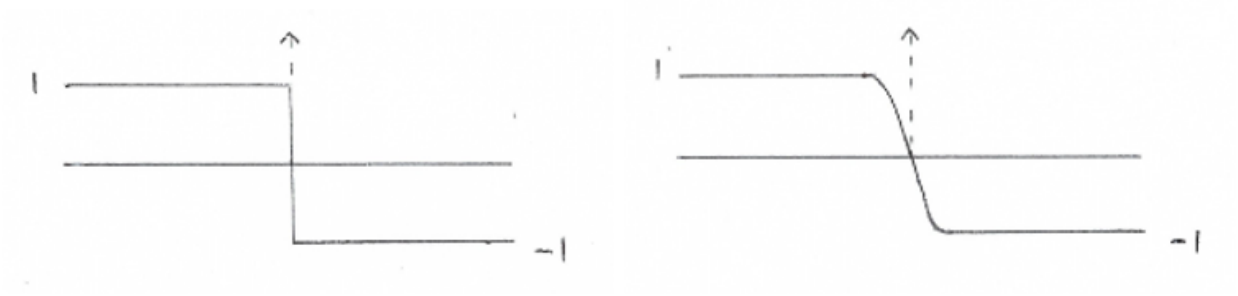

Figure 3.8: f Factor Behavior: Original (Left) and Soft (Right)

regime and the backward regime separately, it was theorized that by skipping the transition between the two, the solver could work correctly in each regime separately. Upon closer inspection of the nature of the singularity, it was found that the singularity was beginning before the nondimensional time reached the point where $\bar{u}_0$ crossed the transition point from positive to negative.

In the case $N = 6$, the solution was going unstable when $\bar{u}_0 < 0.03$, and for $N = 8$, the solution went unstable when $\bar{u}_0 < 0.05$. To skip this zone where the solution went unstable before $\bar{u}_0 = 0$, the solver would stop when $\bar{u}_0 < 0.05$, and then linearly approximate the $\{\bar{\lambda}_n\}$ vector across to $\bar{u}_0 = -0.05$. It would then use approximated $\{\bar{\lambda}_n\}$ as the new initial condition for the section of the solution in the reverse regime. Unfortunately, this stop-start method did not alleviate the instability as the solver continued to expand to infinity after it would skip across the sections where $|\bar{u}_0| < 0.05$.

3.3.4 A New Solver

Because the robust model worked for cases of $N < 5$ states, it was thought that perhaps ode45 was not sophisticated enough to solve how stiff the differential equation was. However after testing all differential solvers provided in MATLAB, as well as an implicit differential equation solver, all solvers tested were still unable to handle cases of $N \geq 5$ without running into the same singularity.

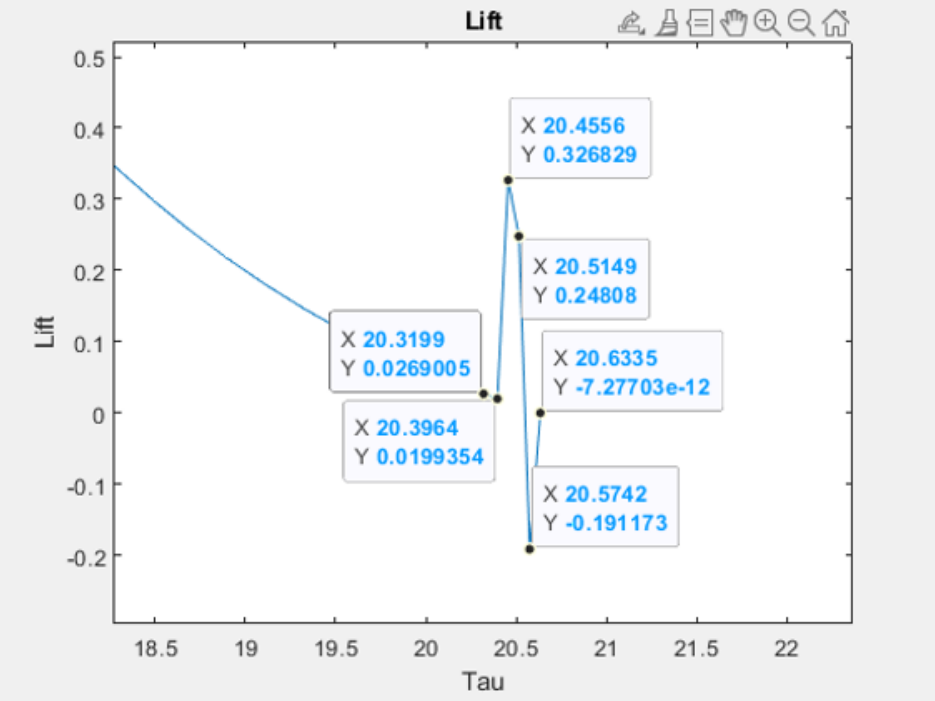

Figure 3.9: Singularity Behavior Just Prior to u_0 Transition

Next, it was theorized that perhaps due to the size of the [A] matrix, the eigenvalues were so large that the solver was losing numerical precision through the jump. All solvers provided by MATLAB maintained double-precision accuracy. As such, a differential equation solver was written from scratch, using a fourth-order Runge-Kutta method as well as MATLAB's variable precision arithmetic (VPA). VPA allows for manual entry of the precision of variables to any specified number of digits. After running the written solver using up to 100 digit precision, it was found there was no difference between the original ode45 results and the new VPA results. It was at this point it was decided that the singularity was not caused by numerical imprecision.

3.3.5 The Modified Free-Stream Method

With numerical errors ruled out, the singularity must be driven by physics. It was hypothesized that as the flow velocity approached zero, there existed a buildup of shed vorticity off

the trailing edge of the airfoil. Since the free-stream here is essentially zero, the vorticity being shed is not being pushed downstream and is creating a concentrated load at that point. This concentrated load would explain the kink in the graphs as the flow crosses zero, as well as why the instability begins before the flow changes direction.

To combat this, a new free-stream velocity model was used in the state-space model, which prevented the flow from going below a set minimum value. The equation for the $\bar{u}_{0Mod}$ can be seen below:

$$\bar{u}_{0Mod} = sign(\bar{u}_0) * \sqrt{\bar{u}_0^2 + \bar{u}_{min}^2} \tag{3.28}$$

The $\bar{u}_{0Mod}$ prevents the free-stream from becoming less than $|\bar{u}_{min}|$, meaning it will instantaneously change from $+\bar{u}_{min}$ to $-\bar{u}_{min}$ when $\bar{u}_0$ would have normally crossed 0 without the modification. Because $\bar{u}_{0Mod}$ never approaches 0, the shed vorticity will always be pushed downstream, preventing it from building up into a concentrated load. A visualization of $\bar{u}_{0Mod}$ is shown below.

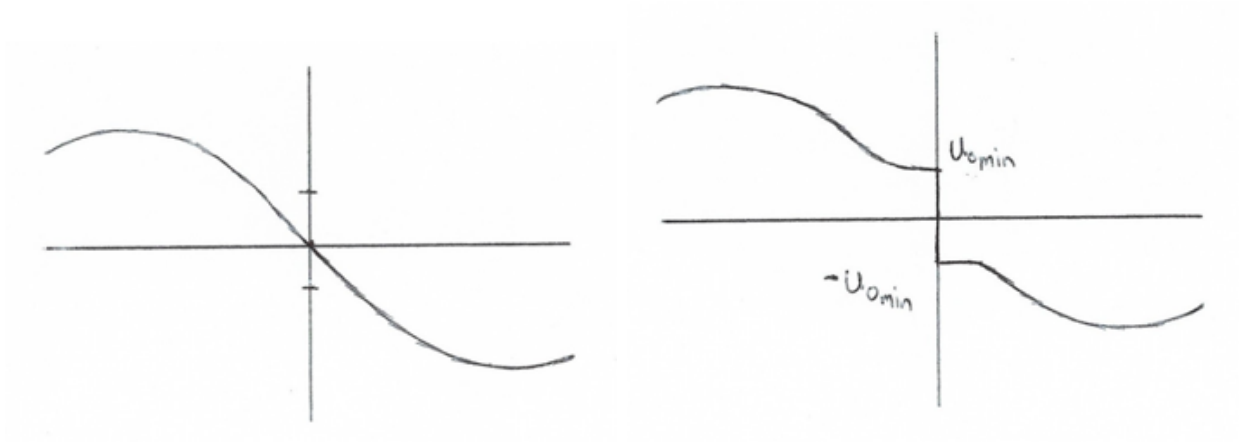

Figure 3.10: Free-Stream (Left) and Modified Free-Stream (Right) Visualization

After implementing $\bar{u}_{0Mod}$ with $\bar{u}_{min} = 0.05$ into the model, it was found that macroscopically there was little difference between the $\bar{u}_0$ and $\bar{u}_{0Mod}$ method on the lift. Upon close inspection however, it was seen that the $\bar{u}_{0Mod}$ method delayed the start point for the instability from what would have normally been $\bar{u}_0 < 0.03$ to $\bar{u}_0 = 0$ for the case of $N = 6$,

	648	649	650	651	652	653	654	655	656	657	658
Old λ_0	-0.5747	-0.5768	-0.5789	-3.7936	-12.4415	-18.3722	-15.5710	-0.5726	27.5386	67.1286	4.6814e+03
New λ_0	-0.5728	-0.5748	-0.5768	-0.5788	-0.5808	-0.5828	-0.5848	-0.5867	1.5172	1.3001	4.5993e+03
u0	0.0426	0.0381	0.0336	0.0292	0.0248	0.0204	0.0161	0.0118	0.0075	0.0033	-8.9412e-04

Figure 3.11: Delay of Singularity Using $\bar{u}_{0Mod}$ Compared to Original Results

and from $\bar{u}_0 < 0.05$ to $\bar{u}_0 < 0.01$ for $N = 8$. Below is the raw MATLAB data from the original response and using the $\bar{u}_{0Mod}$ method for the case of $N = 8$.

To provide insight into what is being displayed: the bottom row shows the value of $\bar{u}_0$ from index 648 – 658. The index values are directly proportional to time in the simulation, where index 658 is the exact time in which $\bar{u}_0$ becomes 0, signifying the point which the flow transitions from forwards to reverse. The top row shows the value of λ_0 from the original model at the corresponding times. As it can be seen by the red box, the value of λ_0 abruptly jumps at index 651 - signifying the beginning of the singularity. The middle row shows the value of λ_0 using the $\bar{u}_{0Mod}$ method. As can be seen in the green box, the singularity does not occur until index 656. Thus the singularity was delayed using the $\bar{u}_{0Mod}$ method. There is no row showing the true value of $\bar{u}_{0Mod}$ since it would be held constant at 0.05. However, the corresponding indexes representing time for $\bar{u}_{0Mod}$ are represented by the bottom row.

3.3.6 An Unforced Model

Next it was proposed to run an unforced model through the problem areas of $|\bar{u}_0| < 0.05$ to see if that would become unstable or not. This model ran on essentially the same concepts as the start-stop model described before, except instead of using linear interpolation across the problem zone, the model would "turn off" the forcing function by setting the right side of Eq. (3.25) to 0, and then have it "turn on" again after it made it through the problem

area. This simplified unforced model is described here:

$$[A]'\{\bar{\lambda}_n\}^* + f\bar{u}_0(\tau)\{\bar{\lambda}_n\} = 0 \tag{3.29}$$

This method produced promising results, while it still grew in magnitude, it did so at a slower rate than the original model. This can be seen below, as the peaks of the unforced model were lower than those of the original. It also delayed the instability from occurring until $\bar{u}_0 = 0$ for all cases including $N = 8$, which was better than the $\bar{u}_{0Mod}$ method.

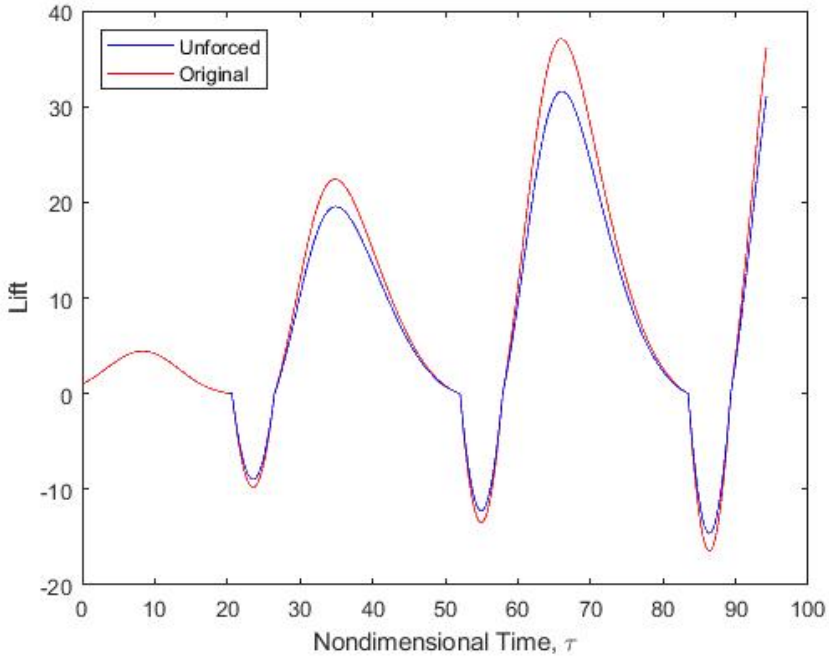

Figure 3.12: Comparison of Original Model to Unforced Stop-Start Model (N = 5)

To examine the long-term periodic nature of the unforced model, the original simulation was run for one period of $\bar{u}_0$. The $\{\bar{\lambda}_n\}$ vector calculated at the end of the period then served as the initial condition of the unforced model, Eq. (3.29). This unforced model was then allowed to run for several more periods to see whether the model would decay to a stable value or expand to infinity. It was discovered that for values of $N \leq 5$, the solution would

decay to a steady state. However for situations of $N > 5$, the solution would expand to infinity.

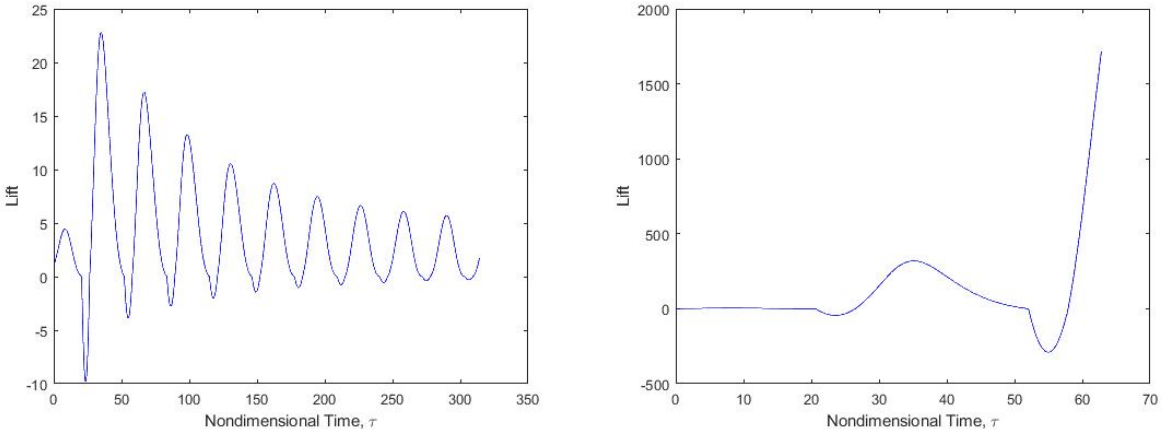

Figure 3.13: Unforced Response with $N = 5$ (Left) and $N = 6$ (Right)

The results of all three tests, the $\bar{u}_{0Mod}$ method, the turn-off and on method, and the complete turn-off method, revealed some very insightful information about the nature of the singularity's occurrence. First, it was hypothesized that the shed vorticity was building up into a concentrated load. The implementation of the $\bar{u}_{0Mod}$ method and the fact that it delayed the instability's occurrence proved that this phenomena was contributing to the singularity. The turn-off and on method showed that the unforced function still went unstable, but with a decreased magnitude, while delaying the instability's occurrence better than the $\bar{u}_{0Mod}$ method. Lastly, the completely unforced model found that the simulation approaches a steady state solution when $N \leq 5$ but still amplifies when $N > 5$. It is believed the cause of this is due to a Floquet instability.

3.3.7 A Floquet Instability

In Peters and Barwey, the time varying inflow was oscillatory, but remained in the forward flow regime for the entirety of the simulation. By changing $\mu > 1$, a time varying periodic

inflow that switches between the forward and backwards flow regimes seems to be the cause of a Floquet instability. This instability did not occur in the forwards regime and as such was never observed previously. Looking at the graphs of the instability in Fig. 3.7, it can be seen that the unstable solution expands in a straight line. This provides more evidence for a Floquet instability since vorticity dies out as a function of $\frac{1}{\tau}$ according to the Biot-Savart Law and the inverse of such would be a straight line.

In an attempt to further confirm the hypothesis of the existence of a Floquet instability, two new free-stream models were developed and tested, both of which involve removing the periodicity of the free-stream equation. In retrospect, a periodic inflow that shifts from forwards to reverse continuously is a phenomena which would most likely never exist in a real world application. It is highly doubtful that a helicopter will be flying up and down or forwards and backwards in an oscillatory manner. Instead, it is more likely that a helicopter will move from flying forwards to flying backwards one single time, or to go forwards-backwards-forwards and continue flying in the forwards direction. The reader could also replace the words “forwards” and “backwards” with “up” and “down” and the scenarios would still apply.

To test these two scenarios, free-stream functions of the following two equations were used to simulate a "Reversal" or "In and Out" motion. The "Reversal" equation maintains a constant forward flow, a smooth transition to reverse flow, followed by constant reverse flow. The "In and Out" equation is a constant forward flow, a dip into reverse flow, followed by a return to constant forward flow.

$$\text{Reversal} \quad \begin{cases} \bar{u}_0 = 1 & 0 < k\tau < 2\pi \\ \bar{u}_0 = cos(k\tau) & 2\pi < k\tau < 3\pi \\ \bar{u}_0 = -1 & k\tau > 3\pi \end{cases} \tag{3.30}$$

$$\text{In and Out} \quad \begin{cases} \bar{u}_0 = 1 & 0 < k\tau < 2\pi \\ \bar{u}_0 = (1 - \frac{\mu}{2}) + \frac{\mu}{2} cos(k\tau) & 2\pi < k\tau < 4\pi \\ \bar{u}_0 = 1 & k\tau > 4\pi \end{cases} \tag{3.31}$$

A visualization of these two free-streams is shown below. In both cases of testing, α was held constant at 1 to eliminate an independent variable.

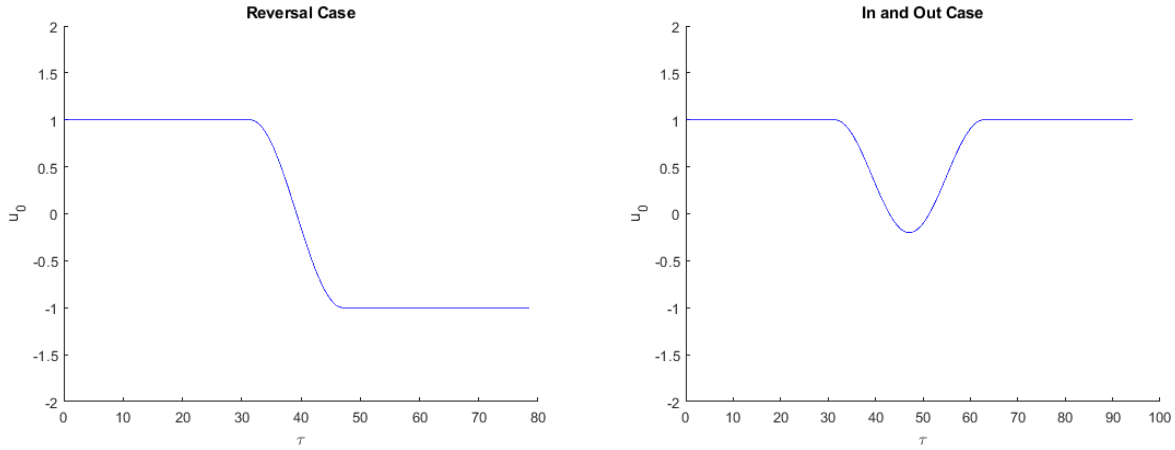

Figure 3.14: Free-Stream Case Visualization

The reversal case produced plots which very quickly spiked in magnitude, but decayed out back to values of -1 with time as the constant free-stream took effect.

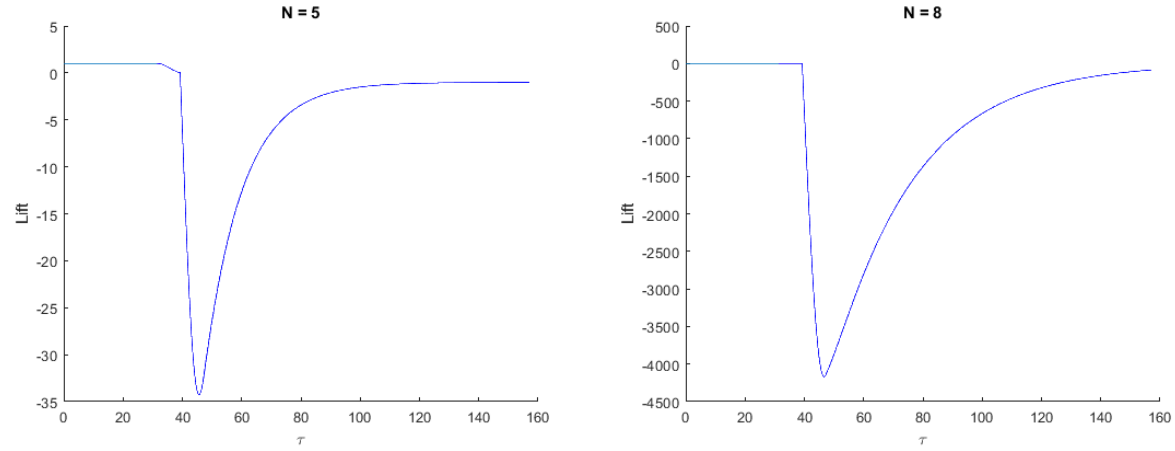

Figure 3.15: Reversal Case Lift Results

Similarly, for the in and out case, the plots quickly spike in magntitude but then settle back to a stable value of 1 as the free-stream remains steady.

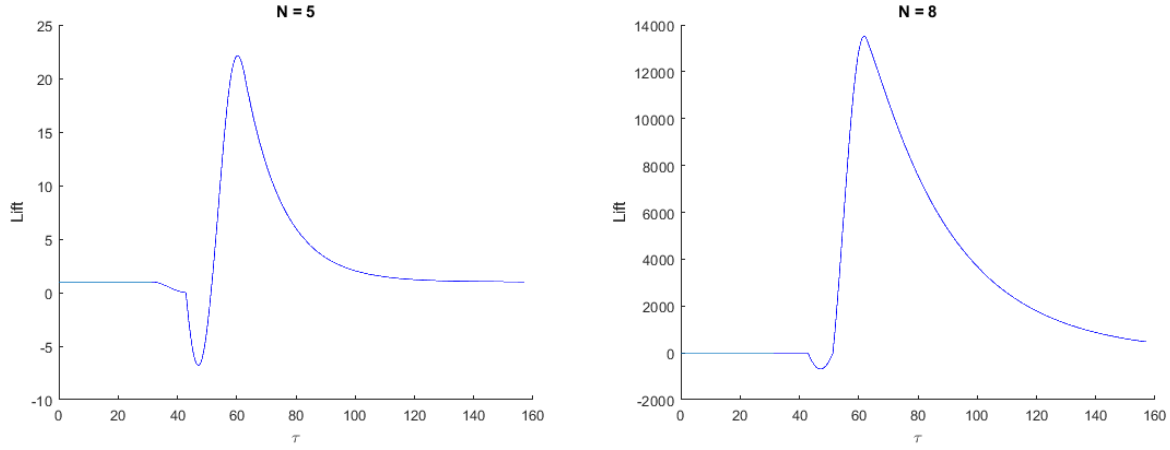

Figure 3.16: In and Out Case Lift Results

Because the reversal case and the in and out case both result in steady state stable responses over the long period, it can be stated with confidence that an oscillatory free-stream which changes direction becomes unstable due to the presence of a Floquet instability. This claim is backed by the fact that Floquet instabilities only exist in periodic systems. The absence of the instability in a system which is non-oscillatory implies that the instability is caused by the oscillatory nature of the system.

A major conclusion, therefore, is that – as the research proceeds to study flow reversal – only one or two flow reversals per case should be considered rather than periodic reversals.

Chapter 4:

Closed-Form Validation of

Finite-State Model

In this section, closed-form results for cases without a Floquet instability are developed, so that they can be used in future validations. In the test case chosen, the equation describing the total bound vorticity for an airfoil in terms of angle of attack (Eqn. (3.7)) is replaced with a specified Γ. The purpose of doing so is to generalize the finite-state model such that any arbitrary geometry can be represented within the model, so long as the user knows the equation for the total bound vorticity that geometry generates.

Since one goal of the project is to extend the effects of changing direction such that the vehicle is capable of flying back into its own wake, the closed-form solution will allow changing the free-stream direction. Up until now the model assumes that once the free-stream changes direction, all shed vortices instantaneously flip to the other side of the airfoil and they are still downstream in the eyes of the free-stream. It is desired to keep these vortices upstream of the geometry so it can fly back into the vortices it has previously shed. This is an important phenomena that occurs in the real world when a helicopter descends back into its own wake.

In order to replace the blade angle of attack time history with that of an arbitrary Γ, the finite-state model will need to be altered and re-derived. Similarly to the reverse model, no previous experimental or theoretical data exists to compare results to. To combat this, a "simple" mathematical equation representing Γ will be chosen. This equation will be simple enough that a closed-from analytic solution for the $\bar{\lambda}_n$'s can be derived using the Biot-Savart

Law. This will provide a lift response with which to compare the finite-state results and determine their validity.

4.1 Derive an Arbitrary Total Bound Vorticity Model

The same equations that derived the the Reverse Flow Model are utilized to generate the Arbitrary Γ Model. These being Eqn. (3.20) – (3.22). The equation for the total bound vorticity of an airfoil, Eqn. (3.19), will be replaced with that of an arbitrary Γ.

Nondimensionalizing the induced flow equations and converting to matrix form while leaving Γ as an arbitrary constant results in the following equation:

$$[A]\{\bar{\lambda}_n\}^* + \bar{u}_0(\tau)\{\bar{\lambda}_n\} = \{c\}\bar{\Gamma}^*/\pi \tag{4.1}$$

This results in a new definition for the [A] and {c} matrices given below:

$$A = \begin{bmatrix} \frac{1}{2}b_1 f & \frac{1}{2}(b_2-1) & \frac{1}{2}b_3 f & \frac{1}{2}b_4 & \frac{1}{2}b_5 f & \frac{1}{2}b_6 & \dots \\ \frac{1}{4} & 0 & -\frac{1}{4} & 0 & 0 & 0 & \dots \\ 0 & \frac{1}{6} & 0 & -\frac{1}{6} & 0 & 0 & \dots \\ 0 & 0 & \frac{1}{8} & 0 & -\frac{1}{8} & 0 & \dots \\ 0 & 0 & 0 & \frac{1}{10} & 0 & -\frac{1}{10} & \dots \\ 0 & 0 & 0 & 0 & \frac{1}{12} & 0 & \dots \\ \vdots & \vdots & \vdots & \vdots & \vdots & \vdots & \ddots \end{bmatrix} \quad c = \begin{bmatrix} f \\ \frac{1}{2} \\ \frac{1}{3}f \\ \frac{1}{4} \\ \frac{1}{5}f \\ \frac{1}{6} \\ \vdots \end{bmatrix} \tag{4.2}$$

It is important to note that the new [A] and {c} matrices are much simpler in form than the original ones in terms of angle of attack. It is also important to recognize that the f factors only exist in the first row of the [A] matrix and in the odd rows of the {c} vector.

4.2 Total Bound Vorticity Representation

Following its derivation, the Arbitrary Γ model was tested in MATLAB. In order to determine the model's validity however, a closed-form representation of a Γ simple enough to solve for lift response analytically was chosen. It is important to note that the governing differential equations for induced flow do not require Γ, they require $\dot{\Gamma}$, and by extension the nondimensionalized $\bar{\Gamma}^*$. Because of this, the Γ "chosen" will just be whichever Γ produces a simple equation for $\bar{\Gamma}^*$.

The $\bar{\Gamma}^*$ chosen is given by:.

$$\bar{\Gamma}^* = T\left(\frac{2\pi}{k} - T\right)\left(\frac{k}{\pi}\right)^2 \tag{4.3}$$

The variable T is constrained by $0 < T < \frac{2\pi}{k}$ and represents the nondimensional distance a fluid particle will travel. This $\bar{\Gamma}^*$ produces a smooth "segment" of vorticity with a length of $\frac{2\pi}{k}$ and a maximum value of 1 occurring at the midpoint. A visualization of the vorticity segment using $k = 0.2$ can be seen below.

4.3 Closed-Form Solution Using Biot-Savart Analysis

4.3.1 Governing Equations of Closed-Form Analysis

In order to solve for the lift due to the vorticity segment in closed-form, it is imperative to define the equations used to do so. The Biot-Savart Law is given by:

$$v = \frac{\Gamma}{2\pi r} \tag{4.4}$$

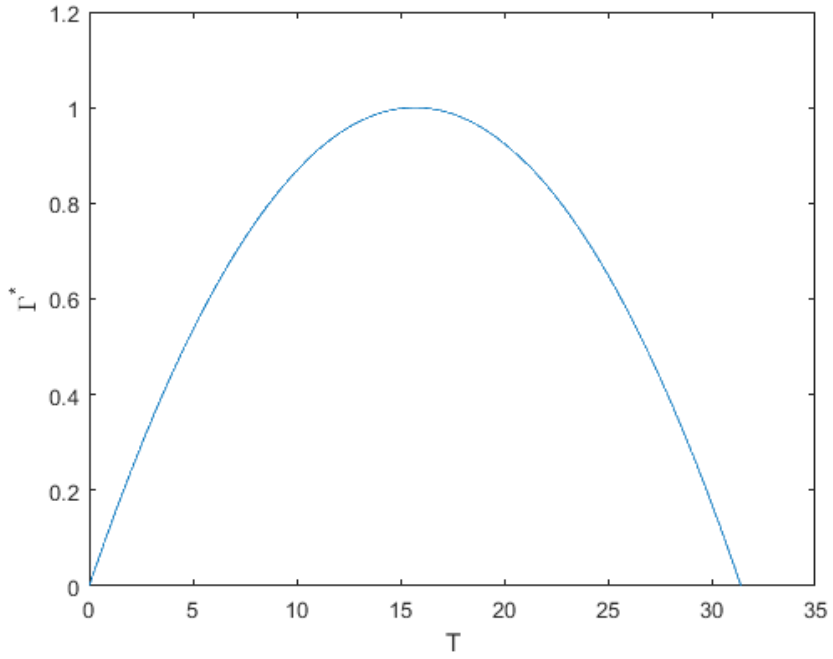

Figure 4.1: Total Bound Vorticity Segment Shape Visualization

Since the segment shape has been defined by $\bar{\Gamma}^*$, the Biot-Savart Law can be re-written as:

$$v = \int \frac{\bar{\Gamma}^*}{2\pi r}\, dr \tag{4.5}$$

Once v is known, Eqn. (4.6) can be used to determine λ_0.

$$\lambda_0 = \frac{1}{\pi}\int_{-b}^{b} \frac{v}{\sqrt{1-x^2}}\, dx \tag{4.6}$$

4.3.2 Gamma-Off Outside Segment Theory

For simplicity, the first case to analyze is that of a vorticity segment which is already fully developed and placed at the trailing edge of the airfoil, which will move downstream with time. Only the homogeneous response to this segment will be solved by setting $\bar{\Gamma}^* = 0$ in the inflow equation. Thus, the only induced flow impinging on the airfoil comes from the

vorticity segment.

Governing Variable Definitions

This analysis is rather complex in its definition and thus it is important to clarify the variable definitions and their relationship to the segment's geometry and the airfoil. Below is a visualization of the Gamma-Off vorticity segment in reference to the airfoil. All distances are nondimensional. T describes the distance by which the vorticity segment is constrained. r represents distance along the x axis beginning from the trailing edge of the airfoil.

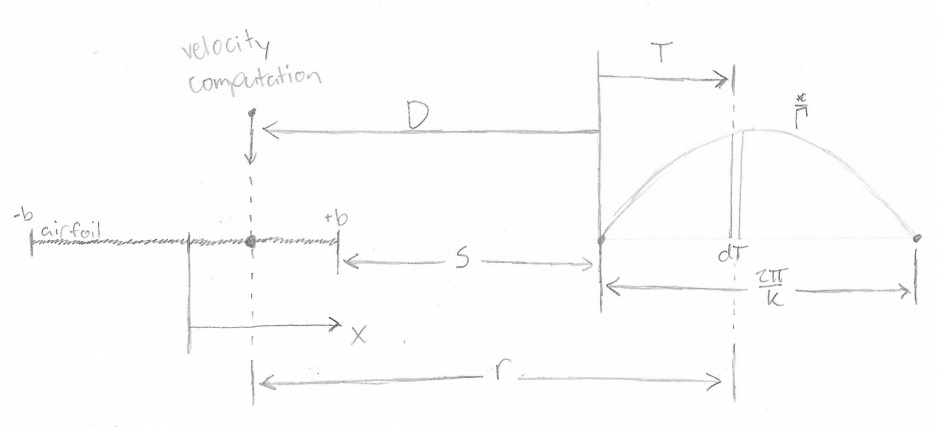

Figure 4.2: Outside Segment Gamma-Off Geometry Visualization and Coordinate Definitions

Closed-Form Induced Flow Derivation

Beginning with the integral version of the Biot-Savart Law, the integral bounds can be described as:

$$v = \int_{D}^{D+T_1} \frac{\bar{\Gamma}^*}{2\pi r}\, dr \tag{4.7}$$

Eqn. (4.7) describes the induced flow at location D. T_1 describes the endpoint of the vorticity segment, or in this case, $\frac{2\pi}{k}$.

Next, because $d\bar{\Gamma} = \bar{\Gamma}^* dT$, a change of variable of $r = T + D$ is made to convert the

integral to:

$$v = \int_0^{\frac{2\pi}{k}} \frac{\bar{\Gamma}^*}{2\pi(T+D)}\, dT \tag{4.8}$$

Allowing the definition of $\bar{\Gamma}^*$ from Eqn. (4.3) to be substituted into Eqn. (4.8) resulting in the following two integrals:

$$v = \left[\frac{k}{\pi^2}\int_0^{\frac{2\pi}{k}} \frac{T}{T+D}\, dT\right] - \left[\frac{k^2}{2\pi^3}\int_0^{\frac{2\pi}{k}} \frac{T^2}{T+D}\, dT\right] \tag{4.9}$$

To evaluate these integrals, the following two indefinite integral definitions were taken directly from Ref. [4].

$$\int \frac{x}{ax+b}\, dT = \frac{x}{a} - \frac{b}{a^2}\ln|ax+b| + C \tag{4.10}$$

$$\int \frac{x^2}{ax+b}\, dT = \frac{1}{a^3}\left[\frac{1}{2}(ax+b)^2 - 2b(ax+b) + b^2\ln|ax+b|\right] + C \tag{4.11}$$

Using these two integral definitions and modifying them such that $a = 1$ and $b = D$ to match the conditions in Eqn. (4.9), the following final result for induced flow due to the vorticity segment is given. A complete derivation showing intermediate steps is provided in the Appendix.

$$v = \frac{1}{\pi} + \frac{kD}{\pi^2}\left[1 - \left(1 + \frac{kD}{2\pi}\right)\ln\left|\frac{2\pi}{kD} + 1\right|\right] \tag{4.12}$$

Closed-Form λ_0 Derivation

With an expression for the induced flow developed, the next step is to find an expression for the average induced flow over the airfoil, λ_0. The definition of λ_0 is given by Eqn. (4.6). Similar to the induced flow, a change of variable must be made to solve the integral. Fig. 4.2 shows the coordinate definitions used to change variables.

Re-writing the λ_0 definition using $x = D - s - b$ results in the following equation. The

integral bounds have been changed from $-b \to b$ to $s \to s + 2b$.

$$\lambda_0 = \frac{1}{\pi} \int_s^{s+2b} \frac{v(D)}{\sqrt{1 - (D - s - b)^2}} \, dD \tag{4.13}$$

This equation was was instead integrated numerically in MATLAB using the trapezoidal method.

4.3.3 Gamma-Off Outside Segment Motion Results

Closed-Form Results

In order to plot Eqn. (4.12) and by extension Eqn. (4.13), values must be chosen for k and D. Similar to the previous chapter, a value of $k = 0.2$ is used in all subsequent analyses. In this chapter the value of $\frac{2\pi}{k}$ is the length of one vorticity segment. Plotting Eqn. (4.12) for three vorticity segment lengths ($0 < D < 3 \times \frac{2\pi}{k}$) gives the following results.

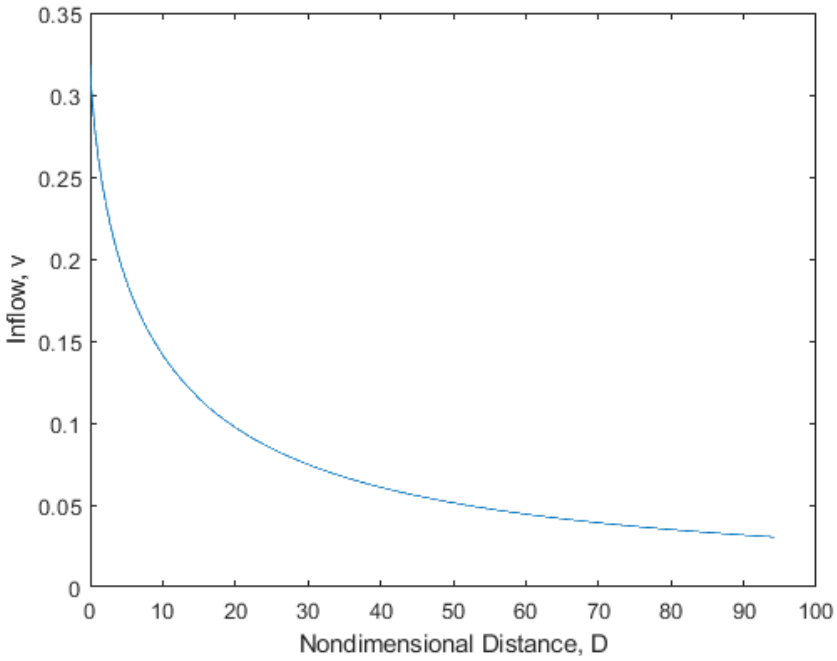

Figure 4.3: Closed-Form Gamma-Off Induced Flow Results

To validate the closed-form response a sanity check was performed. At large D, the vorticity segment should behave like that of a concentrated vortex in reference to its effect on the airfoil. It was calculated that the total vorticity within the segment is:

$$\Gamma = \frac{4}{3}\left(\frac{\pi}{k}\right)^2 \tag{4.14}$$

Applying the Biot-Savart Law shows that at large D, the induced velocity generated by the segment should approach that of a concentrated vortex:

$$v = \frac{2\pi}{3k^2(D + \frac{\pi}{k})} \tag{4.15}$$

Plotting Eqn. (4.12) against Eqn. (4.15) for 100 segment lengths gives the results shown below.

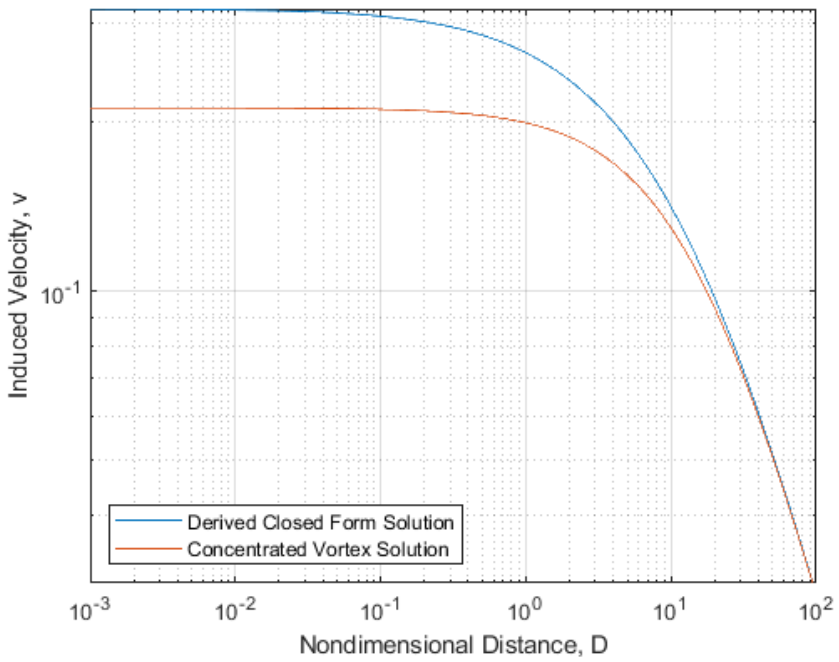

Figure 4.4: Closed-Form Sanity Check Results

Since the two equations converge for large D, it is verified that Eqn. (4.12) is correct.

Finite-State Results

Similarly to the finite-state results presented in the previous chapter, the model was used in conjunction with ode45 to find a time history of the response. As before, initial conditions for the $\{\bar{\lambda}_n\}$ vector were set to 0. Previously, the solver was run for several periods of $\bar{u}_0$ in order to allow transients to dissipate. This time, the solver will run one "period" of response for Eqn. (4.1) for a single vorticity segment length $\frac{2\pi}{k}$ with "Gamma-On" using the $\bar{\Gamma}^*$ presented in Eqn. (4.3). It will then switch to the "Gamma-Off" condition while it completes the time history response. The Gamma-On section gives the solver the correct starting point for generating a solution that compares with the closed-form. The Gamma-Off section describes the solution which is compared with that of the closed-form.

It is important to note that, because the solver is being tested with a constant free-stream value of $\bar{u}_0 = 1$, space and time are directly proportional. This is why comparing a time-history generated by the finite-state model to a distance-history given by the closed-form solution is viable.

The complete time history response of the finite-state results are shown below. The bulge on the left side of the plot is the Gamma-On portion to prepare the initial conditions. This segment is omitted when comparing to the closed-form Gamma-Off solution.

After using a trapezoidal numerical integrator to solve for the closed-form λ_0 with Eqn. (4.13), it is possible to compare the finite-state results with the closed-form solution. This is plotted below.

The x-axis has been defined by s, the nondimensional distance between the trailing edge of the airfoil and the leading edge of the vorticity segment. One can see that the finite-state is a good approximation to the exact. Naturally, as more states are added, the finite-state results will converge to the exact. Here, convergence is not of interest as much as how to reverse the free-stream direction. Again it is possible to plot the time history against the

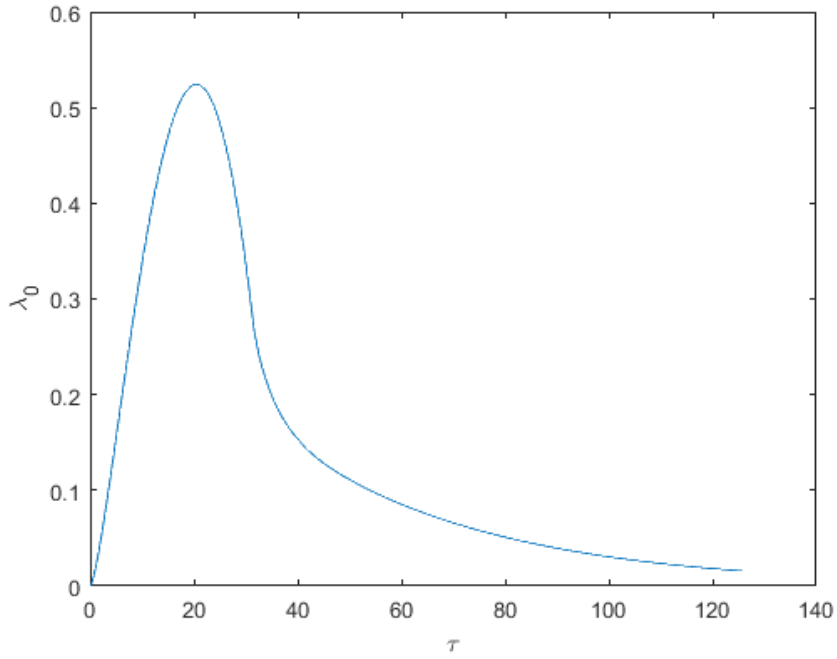

Figure 4.5: Finite-State λ_0 Time History Response – Gamma-Off

distance history because they are equivalent for the case $\bar{u}_0 = 1$. In both plotted solutions, a case of $N = 10$ states was used in the finite-state analysis.

4.3.4 Gamma-Off Inside Segment Theory

As mentioned at the beginning of the chapter, one of the goals of the project is to test the finite-state solver with a vehicle that flies back into its own wake. In order to do this, a closed-form solution must be developed describing the effect of the vorticity segment while it engulfs a portion or the entirety of the airfoil.

Governing Variable Definitions

The visualization of this condition is very similar to that of the outside segment theory, Fig. 4.2, except for the addition of the term ϵ. The singularity at $x = b$ prevents a regular integral from being taken across the vorticity segment. Instead, a Cauchy integral must be

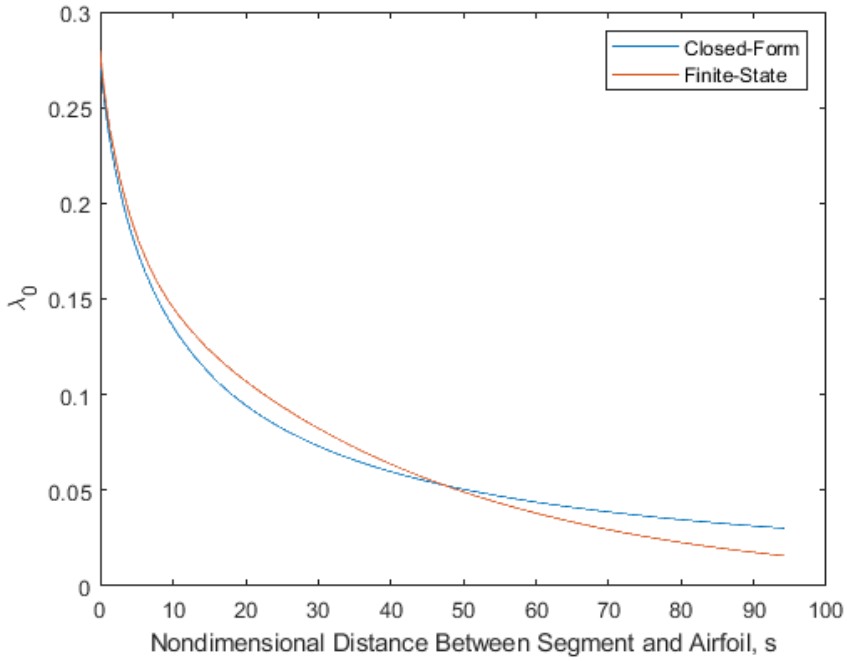

Figure 4.6: λ_0 Comparison of Finite-State Results and Closed-Form Solution

used, with a limit on either side of the singularity. The variable ϵ describes a small distance before or after the integration point. Taking the limit as ϵ approaches 0 will provide the solution of the Cauchy integral.

ϵ describes a small distance either before or after the point at which the vorticity segment is being integrated. It serves as a limit variable in the integration bounds. The Cauchy Integral is defined as:

$$\oint_0^a \frac{1}{x-b}\,dx \equiv \lim_{\epsilon\to 0}\left[-\int_0^{b-\epsilon}\frac{1}{b-x}\,dx + \int_{b+\epsilon}^a \frac{1}{x-b}\,dx\right] \tag{4.16}$$

Where $0 < a < b$.

Below a visualization of the Gamma-Off Inside vorticity segment . The reference is exactly the same as Fig. 4.2 except in the inside case D will be negative.

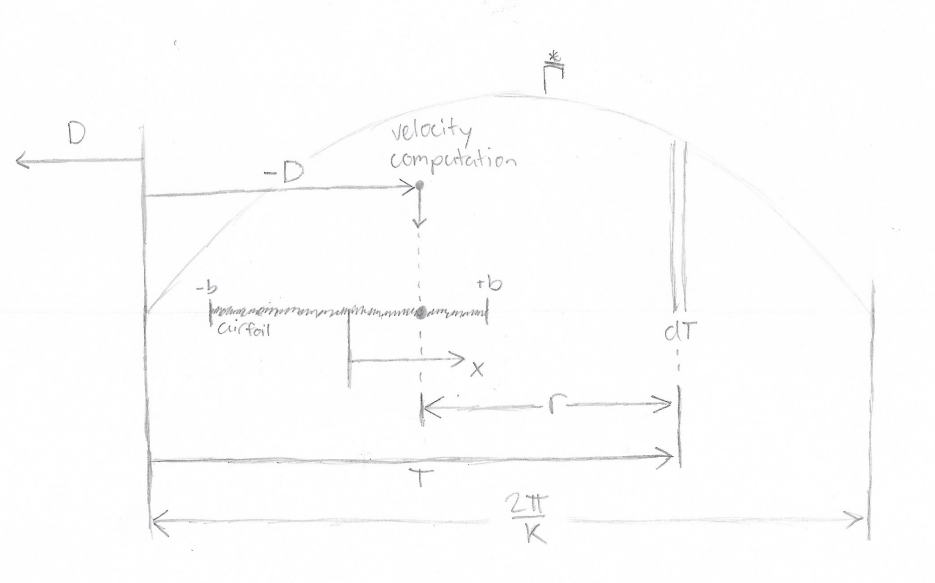

Figure 4.7: Inside Segment Gamma-Off Geometry Visualization and Coordinate Definitions

Closed-Form Induced Flow Derivation

The starting point for the derivation is Eqn. (4.8), the Biot-Savart Law with the change of variable $r = T + D$ subbed in. Applying the Cauchy Integral formula results in Eqn. (4.17).

$$\oint_0^{\frac{2\pi}{k}} \frac{\bar{\Gamma}^*}{2\pi(T+D)}\,dT = \lim_{\epsilon\to 0}\left[-\int_0^{-D-\epsilon} \frac{\bar{\Gamma}^*}{2\pi(-T-D)}\,dT + \int_{-D+\epsilon}^{\frac{2\pi}{k}} \frac{\bar{\Gamma}^*}{2\pi(T+D)}\,dT\right] \tag{4.17}$$

For simplicity solve each integral on the right hand side separately, subbing in the equation for $\bar{\Gamma}^*$ from Eqn. (4.3).

Evaluating the integrals and taking the limit as ϵ goes to 0 results in the final equation for induced flow while inside the vorticity segment:

$$v = \frac{k}{\pi^2}\left[\frac{2\pi}{k} - D\ln\left|\frac{2\pi}{kD}+1\right|\right] + \frac{k^2}{2\pi^3}\left[-\frac{2\pi^2}{k^2} + \frac{2\pi D}{k} - D^2\ln\left|\frac{2\pi}{kD}+1\right|\right] \tag{4.18}$$

Similarly to the outside segment, a complete derivation with intermediate steps can be found in the Appendix.

To solve for λ_0, the same method used in Eqn. (4.13) is used. The only difference is that D is negative.

Future Work

A vorticity segment which returns to engulf the airfoil has yet to be tested. At the moment there are no such data for the closed-form analysis or the finite-state solution, however this section provides a closed-form analytical solution which is prepared to compare to the finite-state solution once it is ready. More on this is presented at the end of this chapter in Section 4.5.

4.3.5 Gamma-On Partial Segment Theory

It is desired to understand the effect of a vorticity segment before it is fully developed by the airfoil. This case will be referred to as Gamma-On since the $\bar{\Gamma}^*$ function is nonzero during this phase.

Governing Variable Definitions

In order to develop an analytic expression for a partial vorticity segment, it is again important to understand the variable definitions and their relationship to the geometry, as it is different from the Gamma-Off case described before. Below is a visualization of the Gamma-On condition at an arbitrary time during the segment's development. As can be seen, most of the variable definitions are similar to those of the Gamma-Off, aside from the addition of the Δ term, which describes the distance the airfoil is "within" the vorticity segment. All the vorticity to the left of the airfoil's trailing edge is "phantom vorticity" as it has yet to be developed. As time moves forwards, the area of the phantom vorticity becomes smaller as the segment moves right with the airflow and continues to be generated. Once the entire

segment has been developed such that $\Delta = 0$, the equations governing the motion of the segment switch over to those of the Gamma-Off condition.

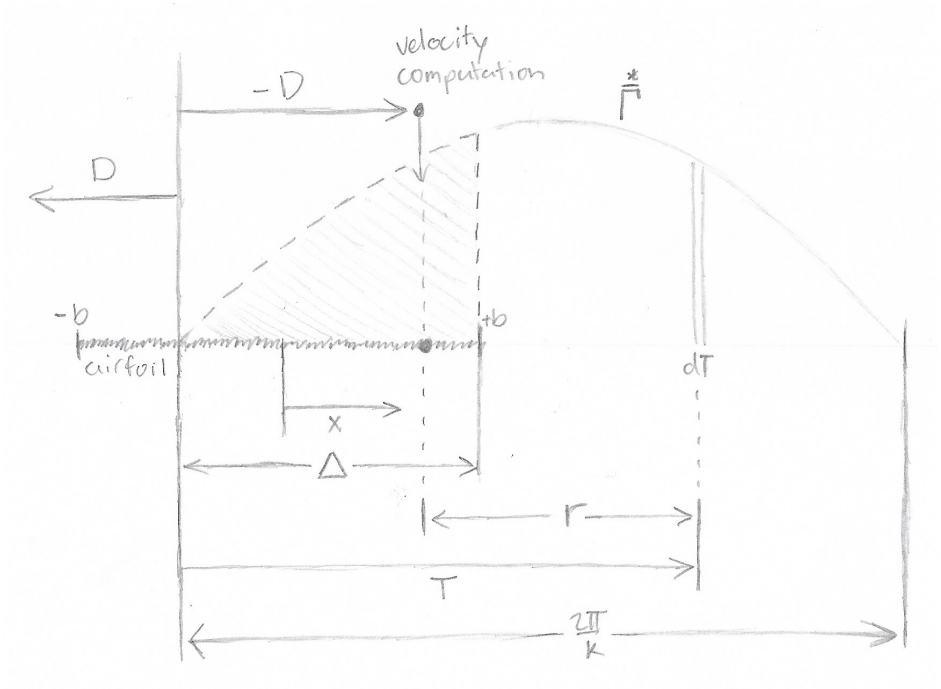

Figure 4.8: Partial Segment Gamma-On Geometry Visualization and Coordinate Definitions

Closed-Form Induced Flow Derivation

Similar to the previous two closed-form derivations, the analysis begins with a modified version of Eqn. (4.8), with the bounds changed to accommodate the partial nature of the segment. This variant is given by:

$$v = \int_{\Delta}^{\frac{2\pi}{k}} \frac{\bar{\Gamma}^*}{2\pi(T+D)}\, dT \tag{4.19}$$

The bounds only go from $\Delta \to \frac{2\pi}{k}$ because the left portion of the segment is nonexistent. Subbing in Eqn. (4.3) and splitting into two integrals gives:

$$\int_{\Delta}^{\frac{2\pi}{k}} \frac{T(\frac{2\pi}{k} - T)\left(\frac{k}{\pi}\right)^2}{2\pi(T+D)}\, dT = \left[\frac{k}{\pi^2}\int_{\Delta}^{\frac{2\pi}{k}} \frac{T}{T+D}\, dT\right] - \left[\frac{k^2}{2\pi^3}\int_{\Delta}^{\frac{2\pi}{k}} \frac{T^2}{T+D}\, dT\right] \tag{4.20}$$

Evaluating the integrals results in the final equation for induced flow due to a partial segment:

$$\begin{aligned} v = \frac{k}{\pi^2}\left[\frac{2\pi}{k} - \Delta + D\ln|\Delta + D| - D\ln\left|\frac{2\pi}{k} + D\right|\right]\ldots \\ + \frac{k^2}{2\pi^3}\left[-\frac{2\pi^2}{k^2} + \frac{2\pi D}{k} + \frac{\Delta^2}{2} - \Delta D - D^2\ln\left|\frac{2\pi}{k} + D\right| + D^2\ln|\Delta + D|\right] \end{aligned} \tag{4.21}$$

A complete derivation with intermediate steps is available in the Appendix.

To check this expression, two conditions can be examined. As mentioned before, when $\Delta \to 0$, the expression should match that of the Gamma-Off Outside Segment. The other is that as $\Delta \to \frac{2\pi}{k}$, the value of v should also go to 0 since the entire segment would exist in the phantom regime. Applying both of these checks does result in the expected results, giving validity to the expression.

An interesting condition to analyze is what happens when $D \to -\Delta$. This is the case for which the infinite inflow from the wake cancels the infinity from the bound vorticity. Thus, the inflow from the wake should be infinite. In order to check this, the value of $D = D + \epsilon$ is substituted into Eqn. (4.21) and then the limit is taken as $\epsilon \to 0$. Sparing the derivation, doing so results in taking the natural log of 0 and sending the value of the expression to ∞.

An Alternate Method

During the course of the development of an expression for λ_0, it was found that there is an alternate method to solve for the value of λ_0 by use of an integral transform method described

in *Helicopter Theory* by Wayne Johnson. The original plan was to develop an expression for λ_0 similar to that of Eqn. (4.13) using the correct bounds and coordinate substitutions that apply to the Gamma-On condition. However, at the time it was theorized that the coordinate transformation method may be able to provide a complete analytical expression for λ_0 since the integrand is easier to integrate after the transformation. This would eliminate the need for numerical integration and provide a more complete expression for the average induced flow over the airfoil. The method and results of doing so are presented next in Section 4.4.

4.4 Closed-Form Solution Using *Helicopter Theory* Integral Transform Method

4.4.1 Governing Equations of Closed-Form Analysis

In his section on Two-Dimensional Unsteady Airfoil Theory from *Helicopter Theory*, Wayne Johnson introduces a conversion for λ_n for Glauert Coefficients in the θ regime to the ξ regime. On page 477 of Ref. [5], he describes the transformation in the following four lines:

$$\begin{aligned}
\lambda_n &= \frac{2}{\pi}\int_0^{\pi} \lambda \cos n\theta \, d\theta \\
&= \frac{2}{\pi}\int_0^{\pi} \left[\frac{1}{2\pi}\int_b^{\infty} \frac{\gamma_w}{x-\xi}\, d\xi\right] \cos n\theta \, d\theta \\
&= -\frac{1}{\pi}\int_b^{\infty} \gamma_w \left[\frac{1}{\pi}\int_0^{\pi} \frac{\cos n\theta}{\xi - b\cos\theta}\, d\theta\right] d\xi \\
&= -\frac{1}{\pi}\int_b^{\infty} \gamma_w \left[\frac{(\xi - \sqrt{\xi^2-b^2})^n}{b^n\sqrt{\xi^2-b^2}}\right] d\xi \qquad \text{[INCORRECT]}
\end{aligned} \tag{4.22}$$

In Eqn. (4.22), the γ_w term describes the wake vorticity function, or $\bar{\Gamma}^*$ for the case of the vorticity segment, and b describes the airfoil half chord as it does in the analysis presented in this paper. It will be shown later that Eqn. (4.22) has a misprint and should include an

additional factor of 2π in the third and fourth lines.

4.4.2 Vorticity Segment Coordinate Transformation

For simplicity, the original coordinate system representation of the segment from Section 4.3 will be referred to as the "T-regime" and the coordinate system using W. Johnson's transformation will be referred to as the "ξ-regime."

Gamma-Off Condition

Below is a visualization of the coordinate transformation between the T and ξ regimes.

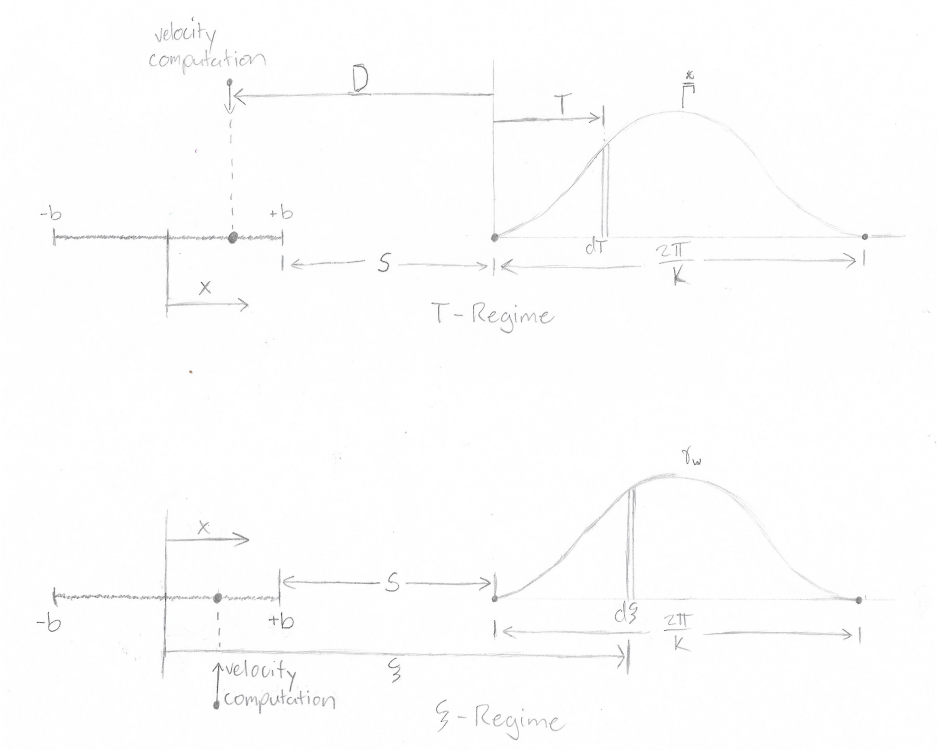

Figure 4.9: Gamma-Off Coordinate Transform Visualization

The following variable definitions exist for the Gamma-Off Condition:

$$T = \xi - s - b$$

$$\xi = T + s + b$$

$$x = -D + s + b$$

$$D = -x + s + b$$

$$x - \xi = -D - T$$

$$\xi - x = D + T$$

The boundaries on the integral of Eqn. (4.22) of $b < \xi < \infty$ describe the area of the entire wake. It is only of concern to calculate the area of the wake such that $\gamma_w \neq 0$. For Gamma-Off this is $0 < T < \frac{2\pi}{k}$ in the T regime. Applying the variable definitions from above:

$$0 < T < \frac{2\pi}{k}$$

$$0 < \xi - s - b < \frac{2\pi}{k}$$

$$s + b < \xi < \frac{2\pi}{k} + s + b$$

These integral bounds will be applied in the derivation in section 4.4.3.

Gamma-On Condition

Below is a visualization of the coordinate transformation between the T and ξ regimes for the Gamma-On Condition.

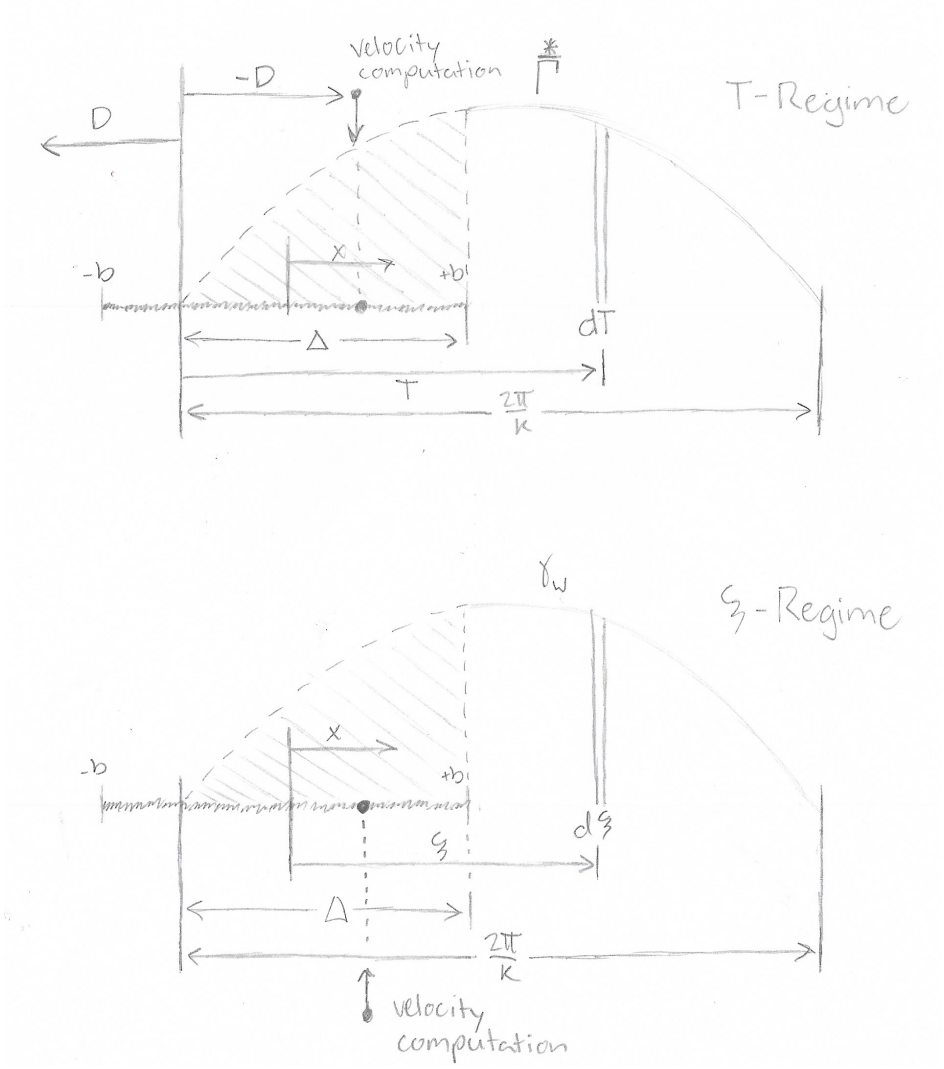

Figure 4.10: Gamma-On Coordinate Transform Visualization

The following variable definitions exist for the Gamma-On condition:

$$T = \xi + \Delta - b$$

$$\xi = T - \Delta + b$$

$$\xi = x$$

$$x = T - \Delta + b$$

$$x = -D - \Delta + b$$

$$D = -x - \Delta + b$$

$$\begin{aligned} x - \xi &= (-D - \Delta + b) - (T - \Delta + b) \\ &= -D - T \\ \xi - x &= D + T \end{aligned}$$

For the Gamma-On condition the nonzero area of the wake is given by $\Delta < T < \frac{2\pi}{k}$ in the T regime. To convert the integral bounds to the ξ regime:

$$\Delta < T < \frac{2\pi}{k}$$

$$0 < \xi + \Delta - b < \frac{2\pi}{k}$$

$$b < \xi < \frac{2\pi}{k} - \Delta + b$$

4.4.3 Closed-Form Induced Flow Derivation in ξ Regime

With the coordinate transformations definitions determined, it is time to apply Eqn. (4.22) to the vorticity segment. To do so, two alterations must be made to Eqn. (4.22).

The first is to divide the $-\frac{1}{\pi}$ coefficient by 2. This is done because Fourier Coefficients of $\frac{2}{\pi} \rightarrow \frac{1}{\pi}$ when $n = 0$. The second is to multiply the entire equation by -1. Looking at line 2 of W. Johnson's Eqn. (4.22), note that the inside integral is defined by the term $\frac{\gamma_w}{x-\xi}$. In the previous analysis in the T regime, the integral was defined by $\frac{\bar{\Gamma}^*}{T+D}$. As shown in Section 4.4.2, in the T regime $x - \xi$ is equivalent to $-D - T$ for both the Gamma-On and Off cases.

Therefore:

$$\frac{\gamma_w}{x-\xi} = \frac{\bar{\Gamma}^*}{-D-T}$$

so the conversion in this case must be such that:

$$\frac{\bar{\Gamma}^*}{D+T} \rightarrow -\left(\frac{\gamma_w}{x-\xi}\right)$$

With both adjustments applied to satisfy the conditions of the previous closed-form analysis, the fourth line of Eqn. (4.22) becomes:

$$\lambda_0 = \frac{1}{2\pi}\int_b^\infty \gamma_w \left[\frac{(\xi - \sqrt{\xi^2-b^2})^n}{b^n\sqrt{\xi^2-b^2}}\right] d\xi \tag{4.23}$$

Apply $n = 0$:

$$\lambda_0 = \frac{1}{2\pi}\int_b^\infty \frac{\gamma_w}{\sqrt{\xi^2-b^2}}\, d\xi \tag{4.24}$$

Eqn. (4.24) expresses λ_0 in the ξ regime. However, the integral bounds will need to be adjusted using the conversions defined in Section 4.4.2.

Gamma-Off Derivation

Begin by substituting the $\bar{\Gamma}^*$ from Eqn. (4.3) into Eqn. (4.24) for γ_w. Alter the integration bounds such that they match those determined for the Gamma-Off condition in Section 4.4.2.

$$\lambda_0 = \frac{1}{2\pi}\int_{s+b}^{\frac{2\pi}{k}+s+b} \frac{\frac{k}{\pi^2}T - \frac{k^2}{2\pi^3}T^2}{\sqrt{\xi^2-b^2}}\, d\xi \tag{4.25}$$

Substitute $T = \xi - s - b$ also from the Gamma-Off portion of Section 4.4.2.

$$\lambda_0 = \frac{1}{2\pi}\int_{s+b}^{\frac{2\pi}{k}+s+b} \frac{\frac{k}{\pi^2}(\xi-s-b) - \frac{k^2}{2\pi^3}(\xi-s-b)^2}{\sqrt{\xi^2-b^2}}\, d\xi \tag{4.26}$$

Expand into multiple integrals:

$$\lambda_0 = \frac{k}{2\pi^3}\left[\int_{s+b}^{\frac{2\pi}{k}+s+b} \frac{\xi}{\sqrt{\xi^2-b^2}} - \frac{s+b}{\sqrt{\xi^2-b^2}}\,d\xi\right]\ldots \\ -\frac{k^2}{4\pi^4}\left[\int_{s+b}^{\frac{2\pi}{k}+s+b} \frac{\xi^2}{\sqrt{\xi^2-b^2}} - \frac{2(s+b)\xi}{\sqrt{\xi^2-b^2}} + \frac{(s^2+2sb+b^2)}{\sqrt{\xi^2-b^2}}\,d\xi\right] \quad (4.27)$$

There are three indefinite integral definitions taken from Ref. [4] which will be used to solve for an expression for λ_0. They are as follows:

$$\int \frac{x}{\sqrt{ax^2+b}}\,dx = \frac{1}{a}\sqrt{ax^2+b} + C \quad (4.28)$$

$$\int \frac{1}{\sqrt{ax^2+b}}\,dx = \frac{1}{\sqrt{a}}\ln|x\sqrt{a}+\sqrt{ax^2+b}| + C \quad (a>0) \quad (4.29)$$

$$\int \frac{x^2}{\sqrt{ax^2+b}}\,dx = \frac{x}{2a}\sqrt{ax^2+b} - \frac{b}{2a\sqrt{a}}\ln|x\sqrt{a}+\sqrt{ax^2+b}| + C \quad (a>0) \quad (4.30)$$

Using these three integral definitions with $a = 1$ and $b = (-b^2)$ gives the following final result for an expression for λ_0. A complete derivation with intermediate steps is provided in the Appendix.

$$\lambda_0 = \frac{k}{2\pi^3}\left[\mathbf{A}-\mathbf{B}+(s+b)\ln\left|\frac{s+b+\mathbf{B}}{\frac{2\pi}{k}+s+b+\mathbf{A}}\right|\right]\ldots \\ +\frac{k^2}{4\pi^4}\left[\frac{(s+b)\mathbf{B}}{2} - \frac{(\frac{2\pi}{k}+s+b)\mathbf{A}}{2} + \frac{b^2}{2}\ln\left|\frac{s+b+\mathbf{B}}{\frac{2\pi}{k}+s+b+A}\right| + 2(s+b)(\mathbf{A}-\mathbf{B})\ldots\right] \\ \left[\ldots + (s^2+b^2+2sb)\ln\left|\frac{s+b+\mathbf{B}}{\frac{2\pi}{k}+s+b+\mathbf{A}}\right|\right] \quad (4.31)$$

Where **A** and **B** are defined as:

$$\mathbf{A} = \sqrt{\frac{4\pi^2}{k^2} + s^2 + 2sb + \frac{4\pi}{k}(s+b)}$$
$$\mathbf{B} = \sqrt{s^2 + 2sb}$$

Gamma-On Derivation

Begin by again substituting the $\bar{\Gamma}^*$ from Eqn. (4.3) into Eqn. (4.24) for γ_w. This time when changing the integration bounds use those defined for the Gamma-On condition from Section 4.4.2.

$$\lambda_0 = \frac{1}{2\pi} \int_b^{\frac{2\pi}{k}-\Delta+b} \frac{\frac{k}{\pi^2}T - \frac{k^2}{2\pi^3}T^2}{\sqrt{\xi^2 - b^2}}\, d\xi \tag{4.32}$$

Substitute $T = \xi + \Delta - b$ from the Gamma-On portion of Section 4.4.2.

$$\lambda_0 = \frac{1}{2\pi} \int_b^{\frac{2\pi}{k}-\Delta+b} \frac{\frac{k}{\pi^2}(\xi+\Delta-b) - \frac{k^2}{2\pi^3}(\xi+\Delta-b)^2}{\sqrt{\xi^2 - b^2}}\, d\xi \tag{4.33}$$

Expand into multiple integrals:

$$\lambda_0 = \frac{k}{2\pi^3}\left[\int_{s+b}^{\frac{2\pi}{k}-\Delta+b} \frac{\xi}{\sqrt{\xi^2-b^2}} + \frac{(\Delta-b)}{\sqrt{\xi^2-b^2}}\, d\xi\right] \ldots$$
$$- \frac{k^2}{4\pi^4}\left[\int_{s+b}^{\frac{2\pi}{k}-\Delta+b} \frac{\xi^2}{\sqrt{\xi^2-b^2}} + \frac{2(\Delta-b)\xi}{\sqrt{\xi^2-b^2}} + \frac{(\Delta^2 - 2\Delta b + b^2)}{\sqrt{\xi^2-b^2}}\, d\xi\right] \tag{4.34}$$

Applying the three integral definitions of Eqns. (4.28) – (4.30) with $a = 1$ and $b = (-b^2)$ results in the final expression for Gamma-On λ_0:

$$\lambda_0 = \frac{k}{2\pi^3}\left[\mathbf{C} + (\Delta - b)\ln\left|\frac{\frac{2\pi}{k} - \Delta + b + \mathbf{C}}{b}\right|\right]\ldots$$
$$+ \frac{k^2}{4\pi^4}\left[\frac{b^2}{2}\ln\left|\frac{b}{\frac{2\pi}{k} - \Delta + b + \mathbf{C}}\right| - \frac{(\frac{2\pi}{k} - \Delta + b)\mathbf{C}}{2} - 2(\Delta - b)\mathbf{C}\ldots\right]$$
$$\left[\cdots + (\Delta^2 - 2\Delta b + b^2)\ln\left|\frac{b}{\frac{2\pi}{k} - \Delta + b + \mathbf{C}}\right|\right] \quad (4.35)$$

Where $\mathbf{C}$ is defined by:

$$\mathbf{C} = \sqrt{\frac{4\pi^2}{k^2} + \frac{4\pi}{k}(b - \Delta) + \Delta^2 - 2\Delta b}$$

A full derivation with intermediate steps is given in the Appendix.

4.4.4 Integral Tranform Method Results

The transform found in *Helicopter Theory* provided an analytical expression for λ_0 for both the Gamma-Off and On conditions. The expressions however, have yet to be verified as correct representations of the average induced flow over the airfoil. Fortunately closed-form results for λ_0 have already been generated for the Gamma-Off condition and were presented earlier in Section 4.3.3.

Gamma-Off Results

The following figure shows the results of plotting the T-regime Gamma-Off closed-form results of Section 4.3.3 against those of the expression derived in the ξ-regime in Section 4.4.3.

Strikingly apparent is the fact that these two closed-form solutions are not in fact equiv-

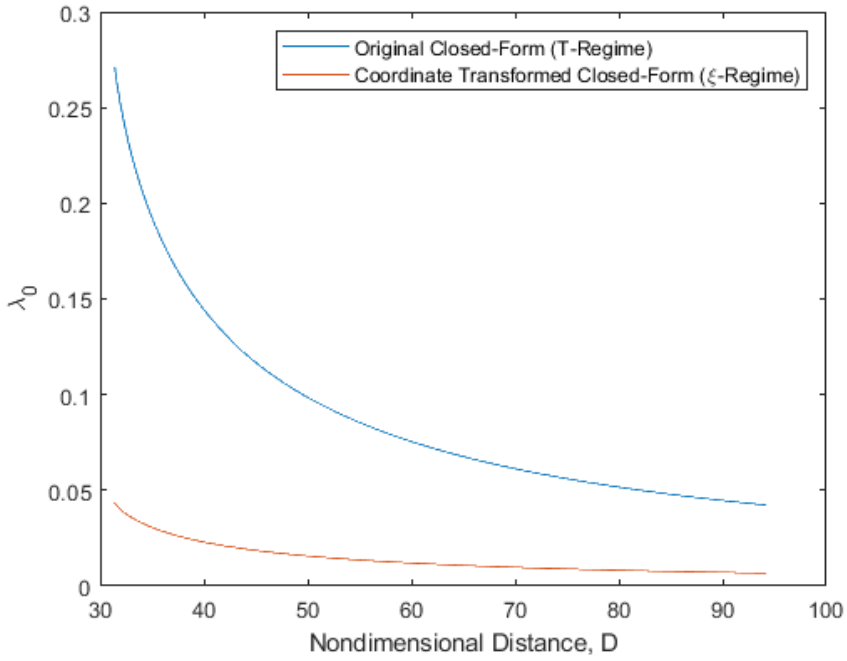

Figure 4.11: Closed-Form Gamma-Off Result Comparison

alent, seemingly ruining the validity of W. Johnson's coordinate transform method as a valid way of representing λ_0 for the vorticity segment. However with some troubleshooting, it was discovered that multiplying Eqn. (4.31) by a factor of 2π results in an expression which exactly matches that of the original from the T-regime. This can be seen in the next figure.

Gamma-On Results

Plotting the Gamma-On results of Eqn. (4.35) in conjunction with the Gamma-Off results before the 2π factor is multiplied shows a smooth transition for λ_0 from Gamma-On to Gamma-Off, which is expected since it describes the development of the vorticity segment into the motion of the segment as it moves away from the airfoil. This smooth transition can be seen in Fig. 4.13.

Similarly multiplying the Gamma-On expression by a factor of 2π and plotting it with the other closed-form solutions results in a smooth transition into the Gamma-Off condition.

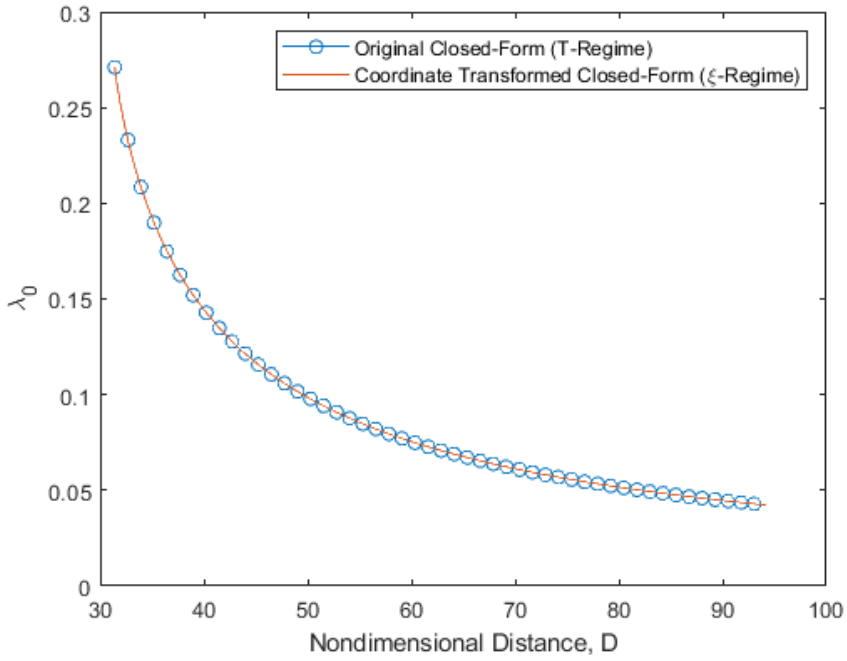

Figure 4.12: Closed-Form Gamma-Off Result Comparison After 2π Adjustment

After paying scrupulous attention to the derivations of the Gamma-On and Off expressions in the ξ-regime presented in Section 4.4.3, it was determined that a typographical error in Ref. [5] results in the missing 2π.

As such, the true final equation for Gamma-Off λ_0 is:

$$\lambda_0 = \frac{k}{\pi^2}\left[\mathbf{A} - \mathbf{B} + (s+b)\ln\left|\frac{s+b+\mathbf{B}}{\frac{2\pi}{k}+s+b+\mathbf{A}}\right|\right]\ldots$$
$$+\frac{k^2}{2\pi^3}\left[\frac{(s+b)\mathbf{B}}{2} - \frac{(\frac{2\pi}{k}+s+b)\mathbf{A}}{2} + \frac{b^2}{2}\ln\left|\frac{s+b+\mathbf{B}}{\frac{2\pi}{k}+s+b+A}\right| + 2(s+b)(\mathbf{A}-\mathbf{B})\ldots\right]$$
$$\left[\cdots + (s^2+b^2+2sb)\ln\left|\frac{s+b+\mathbf{B}}{\frac{2\pi}{k}+s+b+\mathbf{A}}\right|\right] \quad (4.36)$$

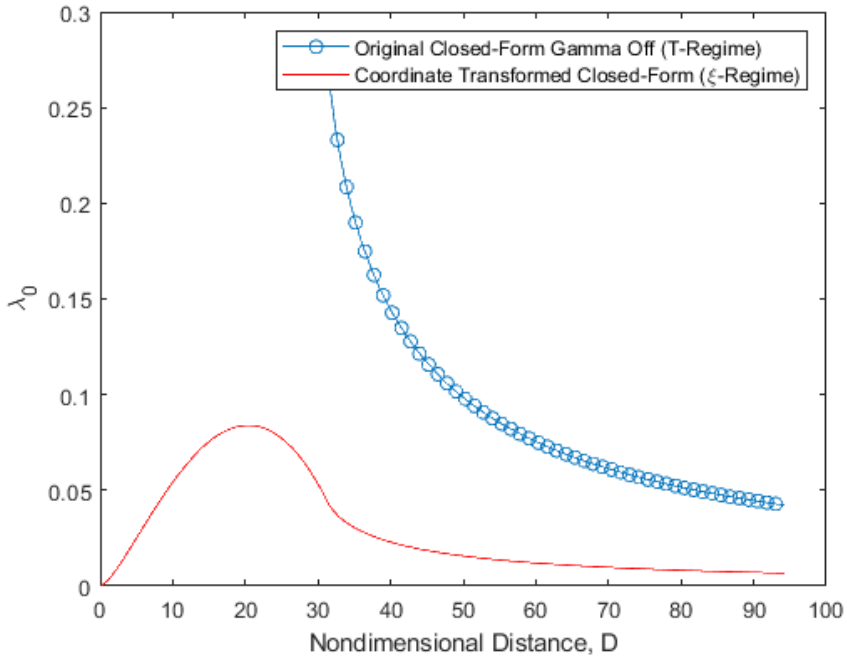

Figure 4.13: Entire Closed-Form Result Comparison

Where **A** and **B** are defined as:

$$\mathbf{A} = \sqrt{\frac{4\pi^2}{k^2} + s^2 + 2sb + \frac{4\pi}{k}(s+b)}$$

$$\mathbf{B} = \sqrt{s^2 + 2sb}$$

And the true final expression for Gamma-On λ_0 is:

$$\lambda_0 = \frac{k}{\pi^2}\left[\mathbf{C} + (\Delta - b)\ln\left|\frac{\frac{2\pi}{k} - \Delta + b + \mathbf{C}}{b}\right|\right]\dots$$
$$+ \frac{k^2}{2\pi^3}\left[\frac{b^2}{2}\ln\left|\frac{b}{\frac{2\pi}{k} - \Delta + b + \mathbf{C}}\right| - \frac{(\frac{2\pi}{k} - \Delta + b)\mathbf{C}}{2} - 2(\Delta - b)\mathbf{C}\dots\right]$$
$$\left[\dots + (\Delta^2 - 2\Delta b + b^2)\ln\left|\frac{b}{\frac{2\pi}{k} - \Delta + b + \mathbf{C}}\right|\right] \quad (4.37)$$

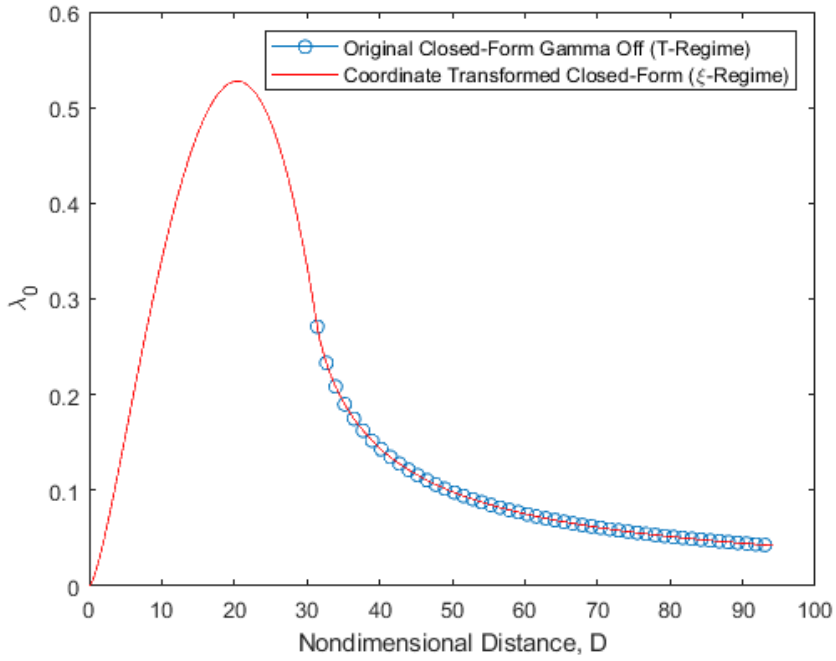

Figure 4.14: Entire Closed-Form Result Comparison After 2π Adjustment

Where $\mathbf{C}$ is defined by:

$$\mathbf{C} = \sqrt{\frac{4\pi^2}{k^2} + \frac{4\pi}{k}(b - \Delta) + \Delta^2 - 2\Delta b}$$

Finite-State Results

Running the finite-state model given by Eqn. (4.1) with initial conditions of 0 for the $\{\bar{\lambda}_n\}$ vector gives the results shown below. These are presented against the closed-form solutions of the coordinate transform method. Changing the number of states results in plots of varying degrees of accuracy compared to the analytic solution.

Based off these results, the finite-state solutions for all 4 cases of N closely approximate the close-form analytic solution for both Gamma-Off and Gamma-On. To determine the

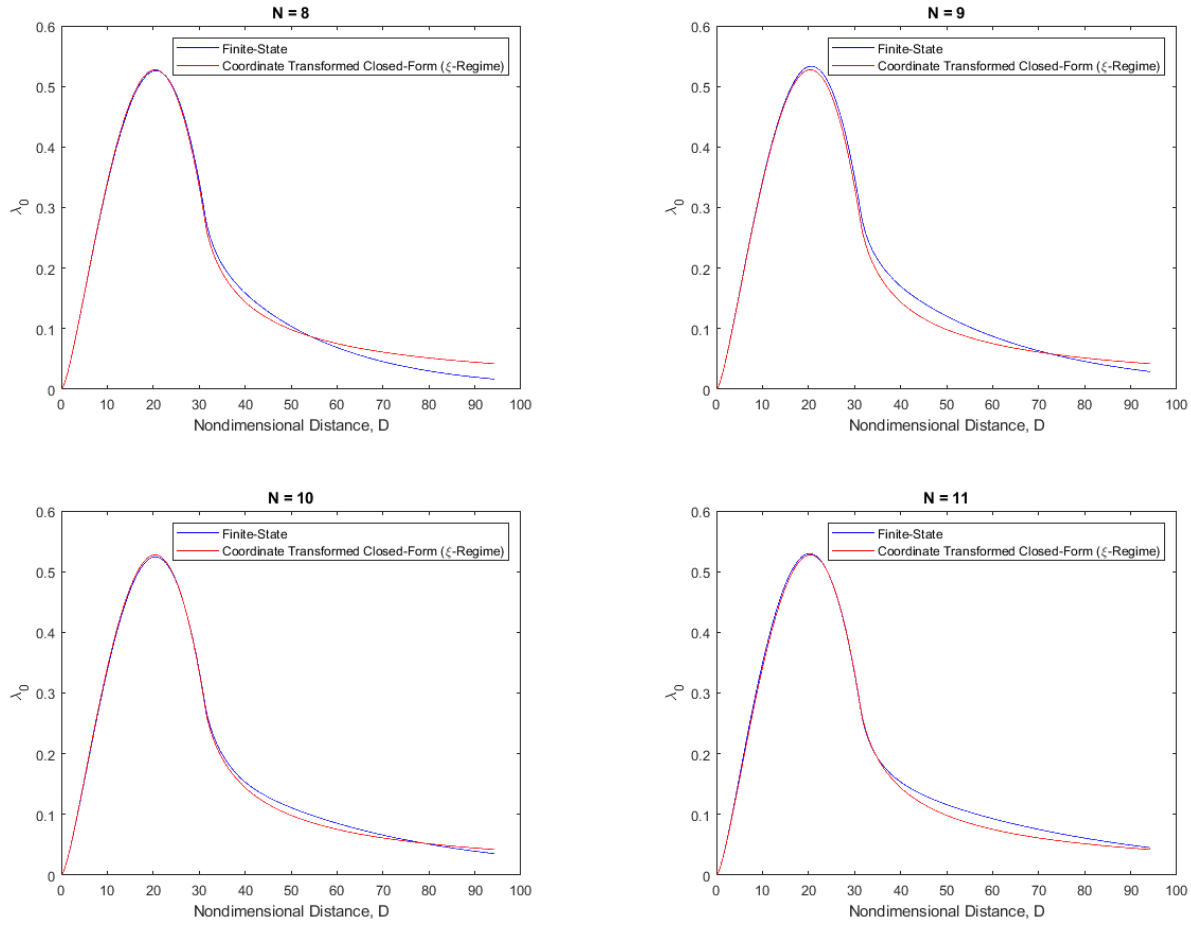

Figure 4.15: Finite-State Results for $N = 8 \rightarrow 11$ Compared with Closed Form Solution

optimal number of states, an error norm was calculated using the following equation:

$$N_{error}^2 = \frac{\sum(\text{Experimental} - \text{Analytic})^2}{\sum \text{Analytic}^2} \tag{4.38}$$

Running the cases of $N = 1 \rightarrow 15$ and plotting the error norm provides the following plot:

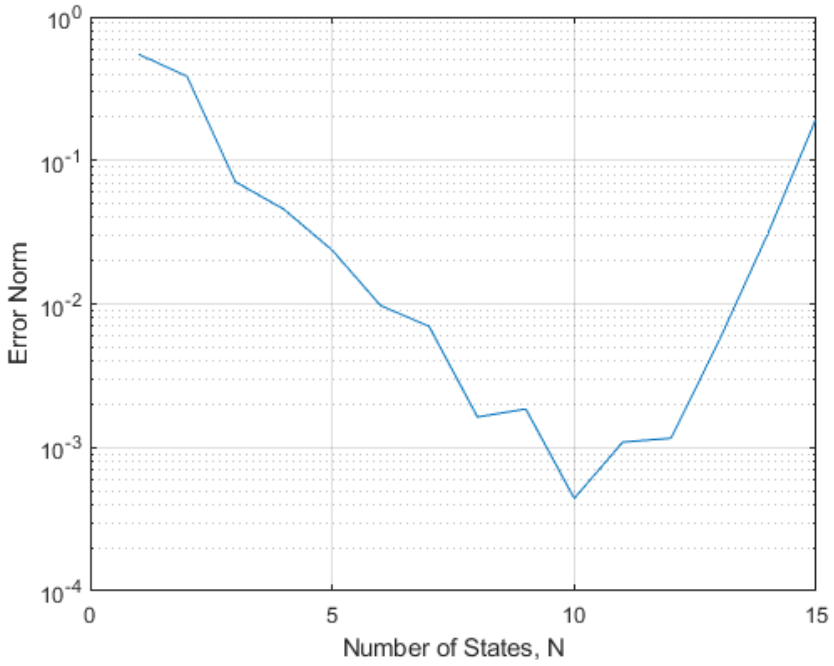

Figure 4.16: Error Norm of Finite-State Solution for $N = 1 \rightarrow 15$

As can be seen, the case of $N = 10$ results in the smallest error norm for the finite-state model and is thus the optimal number of states.

4.5 Future Work

In order to test the Gamma-Off Inside Segment case, time and space must be expressed separately. In all aforementioned analytical analyses, $\bar{u}_0 = 1$, allowing nondimensional time and space to be directly proportional. Because of this, the finite-state results which exist in the time regime could be plotted directly against the closed-form expressions which are

described by nondimensional space. Once the vorticity segment begins moving backwards, meaning that $\bar{u}_0 \neq 1$, the finite-state results can no longer be plotted directly against the distance expressions derived in Section 4.3.4.

In order to bridge the gap of distance and time, an expression to describe nondimensional distance as a function of nondimensional time has been developed. The distance described is that of s, the distance between the vortex segment and the trailing edge of the airfoil. See Fig. 4.2 for a visualization. To describe this distance in terms of time, the following equation has been developed:

$$s = \int_0^{\tau_0} \bar{u}_0 \, d\tau \tag{4.39}$$

Where τ_0 is the time since the Gamma shut-off (which occurs the first time $s = 0$) and $\bar{u}_0 = \frac{u_0}{v_0}$, the free-stream velocity nondimensionalized by the average free-stream velocity.

There will subsequently be three definitions for the value of $\bar{u}_0$ depending on which type of motion the vortex is exhibiting. The vortex will begin by moving away from the airfoil at constant speed similar to the Gamma-Off Outside Segment condition described before. It will then begin slowing down until it stops moving and then accelerates back towards the airfoil before returning to a constant velocity in the negative direction in its third stage.

The three stages are defined as follows:

$$\begin{aligned} \bar{u}_0 &= 1 & 0 < \tau < \tau_1 \\ \bar{u}_0 &= \cos((\tau - \tau_1)k) & \tau_1 < \tau < \tau_2 \\ \bar{u}_0 &= -1 & \tau > \tau_2 \end{aligned}$$

Where τ_1 is the time at which the segment begins slowing down and turning around and $\tau_2 = \tau_1 + \frac{\pi}{k}$ is the time at which the segment stabilizes to a constant negative velocity. It takes $\frac{\pi}{k}$ nondimensional seconds for the segment to decelerate to 0 and accelerate up to -1.

Therefore for the first stage of $0 < \tau < \tau_1$:

$$\begin{aligned} s &= \int_0^{\tau_0} 1 \, d\tau \\ &= \tau_0 \end{aligned} \tag{4.40}$$

For the second stage of $\tau_1 < \tau < \tau_2$:

$$\begin{aligned} s &= \tau_1 + \int_{\tau_1}^{\tau_0} \cos((\tau - \tau_1)k) \, d\tau \\ &= \tau_1 + \frac{1}{k} \sin((\tau_0 - \tau_1)k) \end{aligned} \tag{4.41}$$

For the third stage of $\tau > \tau_2$:

$$\begin{aligned} s &= \tau_1 + \int_{\tau_2}^{\tau_0} (-1) \, d\tau = \tau_1 - \tau_0 + \tau_2 \\ &= 2\tau_1 + \frac{\pi}{k} - \tau_0 \end{aligned} \tag{4.42}$$

The next work to be done in the project will substitute these definitions for s in conjunction with the definitions for Gamma-On and Gamma-Off inside and outside the segment to create a full analytic time history for a vortex segment which is developed, moves away, and then returns and engulfs the airfoil. The closed-form solution will then be compared to the finite-state results to determine the ability of the finite-state model to approximate the effect of a returning wake on an airfoil.

Chapter 5:

Conclusions

5.1 Extensions Using the Mirror Image Approach

Deriving and testing a reverse flow model developed several important conclusions. Firstly, that MATLAB was capable of replicating the results of Peters and Barwey's paper on modelling airloads in an unsteady free-stream using ode45. After modifying the Barwey model into the reverse flow model it was discovered that the model was capable of replicating the original Barwey results in both the forwards and reverse regime. This gave validity to the reverse flow model as a viable method of modelling free-stream flows which move forwards or backwards. However it was subsequently found the model was incapable of handling an unsteady free-stream which changed direction mid-simulation. A singularity occurred at the transition point from forwards to backwards flow causing the response to become unstable.

5.1.1 A Numerical Discrepancy

In an effort to discover and mitigate the source of the singularity, several investigative methods were applied. First, it was theorized the singularity was of numerical origin, and that the solver was merely incapable of numerically integrating through the transition point. To test this theory, first the model was re-written into a more robust form in which the $\{\bar{\lambda}_n\}$ vector never became negative, on the premise that perhaps the change from positive to negative of the $\{\bar{\lambda}_n\}$ vector was the culprit. This was subsequently disproved as the results of the robust model exactly matched those of the original reverse flow model.

Next the reverse flow factor f was changed such that it was a "soft" reverse flow factor

by fitting a smooth curve through its step function. It was thought that perhaps the sharp change of the step function was the cause of the singularity. This however, seemed to have no effect on the development of the singularity.

Next it was hypothesized that removing the transition point altogether could make the response stable, since it was known the model could handle generating a stable response in the forwards and backwards regimes separately. During this inspection it was discovered that the singularity was actually occurring just before the transition point, such that $\bar{u}_0 < 0.05$. By stopping the solver just before this point, linearly interpolating across the transition point, and then using the interpolated point as the initial conditions for the section of the response in the reverse regime, the model skipped the transition point entirely. This also had no effect on the production of the singularity.

Perhaps the solver itself was not sophisticated enough to handle how stiff the model was. As such, all the numerical integrators offered by MATLAB were tested with the model with hopes that the stiff equation solvers could handle the transition point. This also provided fruitless results.

Next it was thought that perhaps the solver was subject to precision error since running the solver with a number of states less than 5 would not produce unstable results. Perhaps double-precision floating point variables were simply not precise enough to handle the 5×5 and 8×8 matrix multiplication being conducted. A differential equation solver was then written from scratch using MATLAB's variable precision arithmetic (VPA) variables, which allows for a user specified number of decimal precision. The solver used a fourth order Runge-Kutta method with a decimal precision of 100 digits, and still did not return results which mitigated the singularity. It was decided at this point that the singularity was not of numerical origin.

5.1.2 A Physics Problem

With numerical issues ruled out, the instability must be caused by physics. Based off the observation of the singularity occurring just before the transition point, it was hypothesized that vorticity was building up at the trailing edge of the airfoil. With essentially zero flow speed, the vorticity being shed from the airfoil is not being pushed downstream and is collecting into a concentrated load.

To test this theory a modified inflow expression was developed such that the free-stream never became stagnant as its value approached 0. This would cause the shed vorticity to be continuously pushed downstream and preventing the buildup. Despite not preventing its occurrence, applying this method resulted in delaying the point at which the singularity appeared, hinting that the vorticity buildup might be partially to blame.

Next it was hypothesized that the forcing function had an effect on the singularity through the transition point. Similarly to the stop-start method, the solver was run in sections, but instead of linearly interpolating through the transition point, the function would be "turned off" by setting the forcing function to 0 and then turning it back on once the transition point had been crossed. Doing so resulted in producing a response which was still unstable but which grew at a slower rate than the original model. A long-term periodic response was also generated by turning off the forcing function after the production of the first period, which produced stable results for the cases of $N < 6$, one more state than the original model.

A Floquet Instability

It was subsequently thought that the cause of the unstable nature of the response is due to a Floquet instability. This was based off the fact that the instability did not occur in a periodic free-stream which flowed only in one direction (like that of Barwey's results) and because the instability growth is linear. According to the Biot-Savart Law, vorticity dies out

as a function of $\frac{1}{\tau}$ and the inverse of such is a straight line, seen in the linear expansion of Fig. 3.7.

To test this theory, two scenarios were developed in which the free-stream would only change direction one time before becoming steady or two times before becoming steady. These cases are actually more practical in nature since it is unlikely that a vehicle such as a helicopter would be changing direction more than twice in any given maneuver. Testing both of these free-stream cases resulted in a response which was stable during the long period. The fact the response did not become unstable after one or two switches in direction lends validity to the existence of a Floquet instability since they can only exist in periodic systems and removing the periodicity of the free-stream erased the instability.

It is the belief of the author and Dr. David A. Peters that the flight of a vehicle in a periodic free-stream which changes direction will result in the production of a Floquet instability. More investigation into this theory should be conducted in the future by other members of the research community to completely verify this hypothesis. If it is true, this research will be the first instance of simulated data describing the existence of a Floquet instability for oscillatory inflows which change direction.

5.2 Closed-Form Comparisons

Following the discovery of a Floquet instability for periodic free-streams which change direction, research shifted to the other goals of the project. One being to replace the total bound vorticity of an airfoil with that of an arbitrary Γ function such that any shape could be used in conjunction with the reverse flow model. The other goal is to study the effect on a vehicle of performing a maneuver in which it flies back into its own wake.

First the finite-state model was re-derived using an arbitrary Γ, with new values for the matrices described. In order to test this model, a closed form analytical expression for λ_0

needed to be developed to compare the finite-state results to. First a simple value for $\bar{\Gamma}^*$ was chosen to make integration by hand easy for comparison. This expression would describe a segment of vorticity which will subsequently be developed, move away from the airfoil, and then return and engulf the airfoil again.

5.2.1 Gamma-Off Outside Segment

First since it involved more simple integration techniques, the case of a fully developed segment (Gamma-Off) placed at the trailing edge of the airfoil which progressively moves away from the edge as it is pushed downstream was analyzed. Using Biot-Savart analysis to solve for induced flow due to the segment's bound vorticity and numerical integration to solve for the average induced flow over the airfoil, two analytical expressions describing v and λ_0 were developed.

These expressions were then plotted against the finite-state results for the same conditions and found that the finite-state model was accurate at approximating the closed-form expressions.

5.2.2 Gamma-Off Inside Segment

Similarly, expressions for v and λ_0 due to a developed segment engulfing the airfoil were also developed. However, the expressions have yet to be tested against finite-state results, so the finite-state model's validity in its own wake has yet to be determined. The reason for the lack of data is that in the case of a segment which returns to the airfoil, nondimensional time and space can no longer be coupled since the value of $\bar{u}_0$ is no longer 1. An expression relating time and space has been developed and presented, it just needs to be applied to the finite-state model and the analytical solution. This will be completed in the near future.

5.2.3 Gamma-On Partial Segment

After an expression was developed for v for the case of a segment which is in the process of being shed from the airfoil (Gamma-On), it was realized that there is another method for determining λ_0 from Wayne Johnson's *Helicopter Theory*, allowing for a closed form analytical expression to be determined instead of having to numerically integrate to find λ_0.

5.2.4 Coordinate Transform Method

In order to use the equations presented in *Helicopter Theory*, the cases of Gamma-On and Gamma-Off (Outside the Segment) had to be converted to the ξ-regime. The transformations for doing this were developed and presented. The case of Gamma-Off while inside the segment was not analyzed as it is believed the transform will not work in the ξ-regime and λ_0 will have to be numerically integrated as before.

Both the Gamma-Off and Gamma-On conditions were derived in the transformed coordinates. Testing them found that both of the expressions were off by a factor of 2π when comparing to the closed form solutions of the previous method using numerical integration for λ_0. It is believed that the discrepancy comes from a typographical error in the book, since the results of the two methods of closed-form analysis do not match. The finite-state results also only approximate the closed-form expressions when they have the 2π factor applied.

Once the factor was applied, it was found that the finite-state model was accurate at approximating the closed-form expressions, validating it as an accurate way of describing an arbitrary bound vorticity for the cases of vorticity development and motion downstream. As mentioned before, vorticity which returns to the airfoil has yet to be tested. Using error-norms it was found that the optimal number of states to describe the segment motion is $N = 10$.

References

[1] Peters, D. A., and Johnson, M. J., "Finite-State Airloads for Deformable Airfoils on Fixed and Rotating Wings," *Proc. of the Symposium on Aeroelasticity and Fluid/Structure Interaction*, Chicago, IL, 1994.

[2] Peters, D. A., Barwey, D., and Johnson, M., "Finite-State Airloads Modeling with Compressibility and Unsteady Free-Stream," *Proc. of the 6th International Workshop on Dynamics and Aeroelastic Stability Modelling of Rotorcraft Systems*, 1995.

[3] Peters, D. A., and Karunamoorthy, S., "State-Space Inflow Models for Rotor Aeroelasticity," *Proc. of the 12th Applied Aerodynamics Conf.*, Colorado Springs, CO, 1994, pp. 828–837.

[4] Hudson, R. G., *The Engineer's Manual*, John Wiley & Sons, Inc., London, England, 1939, Chap. Integral Calculus, pp. 40,43.

[5] Johnson, W., *Helicopter Theory*, Dover Publications, Inc., New York, NY, 1980, Chap. Rotary Wing Aerodynamics I, p. 477.

Appendix

Complete Derivation of Induced Flow Due to Gamma-Off Case While Outside Vorticity Segment

Biot-Savart Law:

$$v = \frac{\Gamma}{2\pi r}$$

Gamma Definition:

$$\Gamma = \Gamma^* dT$$

$$\Gamma^* = T\left(\frac{2\pi}{k} - T\right)\left(\frac{k}{\pi}\right)^2$$

Biot-Savart Integral Form:

$$v = \int_D^{D+T_1} \frac{\Gamma^*}{2\pi r}\, dr$$

Change of variable using $r = T + d$:

$$= \int_0^{\frac{2\pi}{k}} \frac{\Gamma^*}{2\pi(T+D)}\, dT$$

Substitute in Γ^* definition:

$$= \int_0^{\frac{2\pi}{k}} \frac{T\left(\frac{2\pi}{k} - T\right)\left(\frac{k}{\pi}\right)^2}{2\pi(T+D)}\, dT$$

$$= \int_0^{\frac{2\pi}{k}} \frac{\frac{2kT}{\pi} - \frac{T^2k^2}{pi^2}}{2\pi(T+D)}\, dT$$

$$= \int_0^{\frac{2\pi}{k}} \frac{\frac{kT}{\pi^2} - \frac{k^2T^2}{2\pi^3}}{T+D}\, dT$$

$$v = \left[\frac{k}{\pi^2}\int_0^{\frac{2\pi}{k}} \frac{T}{T+D}\,dT\right] - \left[\frac{k^2}{2\pi^3}\int_0^{\frac{2\pi}{k}} \frac{T^2}{T+D}\,dT\right]$$

For simplicity, solve each integral separately. Assign left integral **I** and right integral **II**. Begin with **I**. Use the following indefinite integral definition:

$$\int \frac{x}{ax+b}\,dT = \frac{x}{a} - \frac{b}{a^2}\ln|ax+b| + C$$

Apply to **I** by setting $a = 1$ and $b = D$:

$$\mathbf{I} = \left(\frac{k}{\pi^2}\right)[T - D\ln|T+D|]_0^{\frac{2\pi}{k}}$$

$$= \left(\frac{k}{\pi^2}\right)\left[\frac{2\pi}{k} - D\ln\left|\frac{2\pi}{kD} + D\right| - (-D\ln|D|)\right]$$

$$\mathbf{I} = \frac{2}{\pi} - \frac{Dk}{\pi^2}\ln\left|\frac{2\pi}{kD} + 1\right|$$

Begin **II** with the following indefinite integral definition:

$$\int \frac{x^2}{ax+b}\,dT = \frac{1}{a^3}\left[\frac{1}{2}(ax+b)^2 - 2b(ax+b) + b^2\ln|ax+b|\right] + C$$

Apply to **II** by setting $a = 1$ and $b = D$:

$$\mathbf{II} = \left(\frac{k^2}{2\pi^3}\right)\left[\frac{1}{2}(T+D)^2 - 2d(T+D) + D^2\ln|T+D|\right]_0^{\frac{2\pi}{k}}$$

$$= \left(\frac{k^2}{2\pi^3}\right)\left[\frac{1}{2}\left(\frac{2\pi}{k}+D\right)^2 - 2D\left(\frac{2\pi}{k}+D\right) + D^2\ln\left|\frac{2\pi}{k}+D\right| - \left(\frac{D^2}{2} - 2D^2 + D^2\ln|D|\right)\right]$$

$$= \left(\frac{k^2}{2\pi^3}\right)\left[\frac{1}{2}\left(\frac{4\pi^2}{k^2}+\frac{4\pi D}{k}+D^2\right)-\frac{4\pi D}{k}-2D^2\ldots\right]$$
$$\left[\cdots+D^2\ln\left|\frac{2\pi}{k}+D\right|-\frac{D^2}{2}+2D^2-D^2\ln|D|\right]$$

Consolidate terms:

$$= \left(\frac{k^2}{2\pi^3}\right)\left[\frac{2\pi^2}{k^2}-\frac{2\pi D}{k}+D^2\ln\left|\frac{2\pi}{kD}+1\right|\right]$$

$$\mathbf{II} = \frac{1}{\pi}-\frac{kD}{\pi^2}+\frac{k^2D^2}{2\pi^3}\ln\left|\frac{2\pi}{kD}+1\right|$$

Combine $\mathbf{I}-\mathbf{II}$:

$$= \left[\frac{2}{\pi}-\frac{kD}{\pi^2}\ln\left|\frac{2\pi}{kD}+1\right|\right]-\left[\frac{1}{\pi}-\frac{kD}{\pi^2}+\frac{k^2D^2}{2\pi^3}\ln\left|\frac{2\pi}{kD}+1\right|\right]$$

Final result:

$$v = \frac{1}{\pi}+\frac{kD}{\pi^2}\left[1-\left(1+\frac{kD}{2\pi}\right)\ln\left|\frac{2\pi}{kD}+1\right|\right]$$

Complete Derivation of Induced Flow Due to Gamma-Off Case While Inside Vorticity Segment

Cauchy Integral Definition where $0 < a < b$:

$$\oint_0^a \frac{1}{x-b}\,dx = -\int_0^{1-\epsilon} \frac{1}{b-x}\,dx + \int_{1+\epsilon}^a \frac{1}{x-b}\,dx$$

Biot-Savart Law Integral Form:

$$v = \int_D^{D+T_1} \frac{\Gamma^*}{2\pi r}\,dr$$

Change of variable using $r = T + D$:

$$= \int_0^{\frac{2\pi}{k}} \frac{\Gamma^*}{2\pi(T+D)}\,dT$$

Apply Cauchy Integral Definition:

$$\oint_0^{\frac{2\pi}{k}} \frac{\Gamma^*}{2\pi(T+D)}\,dT = -\int_0^{-D-\epsilon} \frac{\Gamma^*}{2\pi(-T-D)}\,dT + \int_{-D+\epsilon}^{\frac{2\pi}{k}} \frac{\Gamma^*}{2\pi(T+D)}\,dT$$

Substitute in Γ^* definition:

$$= -\int_0^{-D-\epsilon} \frac{T\left(\frac{2\pi}{k}-T\right)\left(\frac{k}{\pi}\right)^2}{2\pi(-T-D)}\,dT + \int_{-D+\epsilon}^{\frac{2\pi}{k}} \frac{T\left(\frac{2\pi}{k}-T\right)\left(\frac{k}{\pi}\right)^2}{2\pi(T+D)}\,dT$$

Describe left integral as **A** and right integral as **B**.

Simplify **A**:

$$\mathbf{A} = \int_0^{-D-\epsilon} \frac{\frac{-2kT}{\pi} + \frac{k^2T^2}{\pi^2}}{2\pi(-T-D)}\,dT$$

$$= -\frac{k}{\pi^2}\int_0^{-D-\epsilon} \frac{T}{-T-D}\,dT + \frac{k^2}{2\pi^3}\int_0^{-D-\epsilon} \frac{T^2}{-T-D}\,dT$$

Call left integral **I** and right integral **II**.

Solve **I** using Eqn. (4.10):

$$-\frac{k}{\pi^2}\int_0^{-D-\epsilon}\frac{T}{2\pi(-T-D)}\,dT = -\frac{k}{\pi^2}\left[-T + D\ln|T+D|\right]_0^{-D-\epsilon}$$

$$= \frac{k}{\pi^2}[-D-\epsilon-D\ln|-D-\epsilon+D| - (-D\ln|D|)]$$

$$= \frac{k}{\pi^2}[-D-\epsilon-D\ln|-\epsilon| + D\ln|D|]$$

$$\mathbf{I} = \frac{k}{\pi^2}[-D-\epsilon-D\ln|\epsilon| + D\ln|D|]$$

Solve **II** using Eqn. (4.11):

$$\frac{k^2}{2\pi^3}\int_0^{-D-\epsilon}\frac{T^2}{2\pi(-T-D)}\,dT = \frac{k^2}{2\pi^3}\left[-\frac{1}{2}(T+D)^2 + 2D(T+D) - D^2\ln|T+D|\right]_0^{-D-\epsilon}$$

$$= \frac{k^2}{2\pi^3}\left[-\frac{1}{2}(-D-\epsilon+D)^2 + 2D(-D-\epsilon+D) - D^2\ln|-D-\epsilon+D|\right]\ldots$$
$$-\frac{k^2}{2\pi^3}\left[-\frac{D^2}{2} + 2D^2 - D^2\ln|D|\right]$$

$$= \frac{k^2}{2\pi^3}\left[-\frac{\epsilon^2}{2} - 2D\epsilon - D^2\ln|-\epsilon| + \frac{D^2}{2} - 2D^2 + D^2\ln|D|\right]$$

$$\mathbf{II} = \frac{k^2}{2\pi^3}\left[-\frac{\epsilon}{2} - 2D\epsilon - \frac{3}{2}D^2 + D^2\ln|D| - D^2\ln|\epsilon|\right]$$

Simplify **B**:

$$\mathbf{B} = \int_{-D+\epsilon}^{\frac{2\pi}{k}}\frac{\frac{2kT}{\pi} - \frac{k^2T^2}{\pi^2}}{2\pi(T+D)}\,dT$$

$$= \frac{k}{\pi^2}\int_{-D+\epsilon}^{\frac{2\pi}{k}}\frac{T}{T+D}\,dT - \frac{k^2}{2\pi^3}\int_{-D+\epsilon}^{\frac{2\pi}{k}}\frac{T^2}{T+D}\,dT$$

Call left integral **III** and right integral **IV**.

Solve **III** using Eqn. (4.10):

$$\frac{k}{\pi^2}\int_{-D+\epsilon}^{\frac{2\pi}{k}} \frac{T}{T+D}\,dT = \frac{k}{\pi^2}[T - D\ln|T+D|]_{-D+\epsilon}^{\frac{2\pi}{k}}$$

$$= \frac{k}{\pi^2}\left[\frac{2\pi}{k} - D\ln\left|\frac{2\pi}{k}+D\right| - ((-D+\epsilon) - D\ln|-D+\epsilon+D|)\right]$$

$$\mathbf{III} = \frac{k}{\pi^2}\left[\frac{2\pi}{k} + D - \epsilon - D\ln\left|\frac{2\pi}{k}+D\right| + D\ln|\epsilon|\right]$$

Solve **IV** using Eqn. (4.11):

$$\frac{k^2}{2\pi^3}\int_{-D+\epsilon}^{\frac{2\pi}{k}} \frac{T^2}{T+D}\,dT = \frac{k^2}{2\pi^3}\left[\frac{1}{2}(T+D)^2 - 2D(T+D) + D^2\ln|T+D|\right]_{-D+\epsilon}^{\frac{2\pi}{k}}$$

$$= \frac{k^2}{2\pi^3}\left[\frac{1}{2}\left(\frac{2\pi}{k}+D\right)^2 - 2D\left(\frac{2\pi}{k}+D\right) + D^2\ln\left|\frac{2\pi}{k}+D\right|\right]\ldots$$
$$- \frac{k^2}{2\pi^3}\left[\frac{1}{2}(-D+\epsilon+D)^2 - 2D(-D+\epsilon+D) + D^2\ln|-D+\epsilon+D|\right]$$

$$= \frac{k^2}{2\pi^3}\left[\frac{1}{2}\left(\frac{4\pi^2}{k^2}+\frac{4\pi D}{k}+D^2\right) - \frac{4\pi D}{k} - 2D^2 + D^2\ln\left|\frac{2\pi}{k}+D\right|\right]\ldots$$
$$- \frac{k^2}{2\pi^3}\left[\frac{\epsilon^2}{2} - 2D\epsilon + D^2\ln|\epsilon|\right]$$

$$= \frac{k^2}{2\pi^3}\left[\frac{2\pi^2}{k^2} + \frac{2\pi D}{k} + \frac{D^2}{2} - \frac{4\pi D}{k} - 2D^2 + D^2\ln\left|\frac{2\pi}{k}+D\right| - \frac{\epsilon^2}{2} + 2D\epsilon - D^2\ln|\epsilon|\right]$$

$$\mathbf{IV} = \frac{k^2}{2\pi^3}\left[\frac{2\pi^2}{k^2} - \frac{2\pi D}{k} - \frac{3D^2}{2} - \frac{\epsilon^2}{2} + 2D\epsilon + D^2\ln\left|\frac{2\pi}{k}+D\right| - D^2\ln|\epsilon|\right]$$

Solve for v by combining $(\mathbf{I}+\mathbf{II})+(\mathbf{III}-\mathbf{IV})$:

$$\mathbf{A}+\mathbf{B}=\frac{k}{\pi^2}\left[-D-\epsilon-D\ln|\epsilon|+\frac{2\pi}{k}+D-\epsilon-D\ln\left|\frac{2\pi}{k}+D\right|+D\ln|\epsilon|\right]\dots$$
$$+\frac{k^2}{2\pi^3}\left[-\frac{\epsilon^2}{2}-2D\epsilon-\frac{3D^2}{2}+D^2\ln|D|-D^2\ln|\epsilon|-\frac{2\pi^2}{k^2}+\frac{2\pi D}{k}+\frac{3D^2}{2}+\frac{\epsilon^2}{2}-2D\epsilon\dots\right]$$
$$\left[\cdots-D^2\ln\left|\frac{2\pi}{k}+D\right|+D^2\ln|\epsilon|\right]$$

$$=\frac{k}{\pi^2}\left[\frac{2\pi}{k}-2\epsilon-D\ln\left|\frac{2\pi}{k}+D\right|+\ln\left|\frac{\epsilon}{\epsilon}\right|\right]\dots$$
$$+\frac{k^2}{2\pi^3}\left[-\frac{2\pi^2}{k^2}+\frac{2\pi D}{k}-4D\epsilon-D^2\ln\left|\frac{2\pi}{k}+D\right|+D^2\ln\left|\frac{\epsilon}{\epsilon}\right|\right]$$

Simplifying and taking the limit as ϵ approaches 0:

$$v=\frac{k}{\pi^2}\left[\frac{2\pi}{k}-D\ln\left|\frac{2\pi}{kD}+1\right|\right]+\frac{k^2}{2\pi^3}\left[-\frac{2\pi^2}{k^2}+\frac{2\pi D}{k}-D^2\ln\left|\frac{2\pi}{kD}+1\right|\right]$$

Complete Derivation of Induced Flow of a Partial Segment Due to Gamma-On Case

Biot-Savart Law Integral Form:

$$v = \int_{D}^{D+T_1} \frac{\Gamma^*}{2\pi r}\, dr$$

Change of variable using $r = T + D$ with integral boundaries applied:

$$= \int_{\Delta}^{\frac{2\pi}{k}} \frac{\Gamma^*}{2\pi(T+D)}\, dT$$

Subbing in Eqn. (4.3) and splitting into two integrals gives:

$$\int_{\Delta}^{\frac{2\pi}{k}} \frac{T(\frac{2\pi}{k} - T)\left(\frac{k}{\pi}\right)^2}{2\pi(T+D)}\, dT = \left[\frac{k}{\pi^2}\int_{\Delta}^{\frac{2\pi}{k}} \frac{T}{T+D}\, dT\right] - \left[\frac{k^2}{2\pi^3}\int_{\Delta}^{\frac{2\pi}{k}} \frac{T^2}{T+D}\, dT\right]$$

Call the left integral **A** and the right **B**, solving each separately.

Integrate **A** using Eqn. (4.10):

$$\frac{k}{\pi^2}\int_{\Delta}^{\frac{2\pi}{k}} \frac{T}{T+D}\, dT = \frac{k}{\pi^2}[T - D\ln|T+D|]_{\Delta}^{\frac{2\pi}{k}}$$

$$= \frac{k}{\pi^2}\left[\frac{2\pi}{k} - D\ln\left|\frac{2\pi}{k} + D\right| - (\Delta - D\ln|\Delta + D|)\right]$$

$$\mathbf{A} = \frac{k}{\pi^2}\left[\frac{2\pi}{k} - \Delta + D\ln|\Delta + D| - D\ln\left|\frac{2\pi}{k} + D\right|\right]$$

Integrate **B** using Eqn. (4.11):

$$\frac{k^2}{2\pi^3}\int_{\Delta}^{\frac{2\pi}{k}} \frac{T^2}{T+D}\, dT = \frac{k^2}{2\pi^3}\left[\frac{1}{2}(T+D)^2 - 2D(T+D) + D^2\ln|T+D|\right]_{\Delta}^{\frac{2\pi}{k}}$$

$$= \frac{k^2}{2\pi^3}\left[\frac{1}{2}\left(\frac{2\pi}{k}+D\right)^2 - 2D\left(\frac{2\pi}{k}+D\right) + D^2\ln\left|\frac{2\pi}{k}+D\right|\ldots\right]$$
$$\left[\cdots - \left(\frac{1}{2}(\Delta+D)^2 - 2D(\Delta+D) + D^2\ln|\Delta+D|\right)\right]$$

$$= \frac{k^2}{2\pi^3}\left[\frac{1}{2}\left(\frac{4\pi^2}{k^2}+\frac{4\pi D}{k}+D^2\right) - \frac{4\pi D}{k} - 2D^2 + D^2\ln\left|\frac{2\pi}{k}+D\right|\ldots\right]$$
$$\left[\cdots - \left(\frac{1}{2}(\Delta^2+2\Delta D+D^2) - 2\Delta D - 2D^2 + D^2\ln|\Delta+D|\right)\right]$$

$$\mathbf{B} = \frac{k^2}{2\pi^3}\left[\frac{2\pi^2}{k^2} - \frac{2\pi D}{k} - \frac{\Delta^2}{2} + \Delta D + D^2\ln\left|\frac{2\pi}{k}+D\right| - D^2\ln|\Delta+D|\right]$$

Solving $(\mathbf{A}-\mathbf{B})$ results in the final equation for induced flow due to a partial segment:

$$v = \frac{k}{\pi^2}\left[\frac{2\pi}{k} - \Delta + D\ln|\Delta+D| - D\ln\left|\frac{2\pi}{k}+D\right|\right]\ldots$$
$$+ \frac{k^2}{2\pi^3}\left[-\frac{2\pi^2}{k^2} + \frac{2\pi D}{k} + \frac{\Delta^2}{2} - \Delta D - D^2\ln\left|\frac{2\pi}{k}+D\right| + D^2\ln|\Delta+D|\right]$$

Complete Derivation of Gamma-Off λ_0 in ξ Regime

Begin with Eqn. (4.24).

$$\lambda_0 = \frac{1}{2\pi}\int_b^\infty \frac{\gamma_w}{\sqrt{\xi^2 - b^2}}\,d\xi$$

Substitute in Γ^* from Eqn. (4.3) for γ_w. Alter the integration bounds such that they match those determined for the Gamma-Off condition in Section 4.4.2.

$$\lambda_0 = \frac{1}{2\pi}\int_{s+b}^{\frac{2\pi}{k}+s+b} \frac{\frac{k}{\pi^2}T - \frac{k^2}{2\pi^3}T^2}{\sqrt{\xi^2 - b^2}}\,d\xi$$

Substitute $T = \xi - s - b$ also from the Gamma-Off portion of Section 4.4.2.

$$\lambda_0 = \frac{1}{2\pi}\int_{s+b}^{\frac{2\pi}{k}+s+b} \frac{\frac{k}{\pi^2}(\xi - s - b) - \frac{k^2}{2\pi^3}(\xi - s - b)^2}{\sqrt{\xi^2 - b^2}}\,d\xi$$

Expand into two integrals:

$$\lambda_0 = \frac{1}{2\pi}\int_{s+b}^{\frac{2\pi}{k}+s+b} \frac{k}{\pi^2}\frac{(\xi - s - b)}{\sqrt{\xi^2 - b^2}}\,d\xi \ldots$$
$$- \frac{1}{2\pi}\int_{s+b}^{\frac{2\pi}{k}+s+b} \frac{k^2}{2\pi^3}\frac{(\xi^2 - 2s\xi - 2b\xi + 2sb + s^2 + b^2)}{\sqrt{\xi^2 - b^2}}\,d\xi$$

Expand left integral and call it **I**, doing the same to the right integral and calling it **II**.

$$\mathbf{I} = \frac{k}{2\pi^3}\int_{s+b}^{\frac{2\pi}{k}+s+b} \left[\frac{\xi}{\sqrt{\xi^2 - b^2}} - \frac{(s+b)}{\sqrt{\xi^2 - b^2}}\right]\,d\xi$$

$$\mathbf{II} = -\frac{k^2}{4\pi^4}\int_{s+b}^{\frac{2\pi}{k}+s+b} \left[\frac{\xi^2}{\sqrt{\xi^2 - b^2}} - \frac{2(s+b)\xi}{\sqrt{\xi^2 - b^2}} + \frac{(s^2 + 2sb + b^2)}{\sqrt{\xi^2 - b^2}}\right]\,d\xi$$

Begin with **I**. Call left integral **1** and right integral **2**. Integrating **1** using Eqn. (4.28) results in:

$$\frac{k}{2\pi^3}\int_{s+b}^{\frac{2\pi}{k}+s+b}\frac{\xi}{\sqrt{\xi^2-b^2}}\,d\xi=\frac{k}{2\pi^3}\left[\sqrt{\xi^2-b^2}\right]_{s+b}^{\frac{2\pi}{k}+s+b}$$

$$=\frac{k}{2\pi^3}\left[\sqrt{\left(\frac{2\pi}{k}+s+b\right)^2-b^2}-\sqrt{(s+b)^2-b^2}\right]$$

$$=\frac{k}{2\pi^3}\left[\sqrt{\frac{4\pi^2}{k^2}+s^2+2sb+\frac{4\pi}{k}}-\sqrt{s^2+2sb}\right]$$

$$\mathbf{1}=\frac{k}{2\pi^3}\left[\mathbf{A}-\mathbf{B}\right]$$

Where **A** and **B** are defined as:

$$\mathbf{A}=\sqrt{\frac{4\pi^2}{k^2}+s^2+2sb+\frac{4\pi}{k}}$$

$$\mathbf{B}=\sqrt{s^2+2sb}$$

Move to integral **2** and integrate with Eqn. (4.29).

$$-\frac{k}{2\pi^3}\int_{s+b}^{\frac{2\pi}{k}+s+b}\frac{(s+b)}{\sqrt{\xi^2-b^2}}\,d\xi=-\frac{k}{2\pi^3}\left[(s+b)\ln\left|\xi+\sqrt{\xi^2-b^2}\right|\right]_{s+b}^{\frac{2\pi}{k}+s+b}$$

$$=-\frac{k}{2\pi^3}(s+b)\left[\ln\left|\frac{2\pi}{k}+s+b+\sqrt{\left(\frac{2\pi}{k}+s+b\right)^2-b^2}\right|-\ln\left|s+b+\sqrt{s^2+2sb}\right|\right]$$

$$=-\frac{k}{2\pi^3}(s+b)\left[\ln\left|\frac{2\pi}{k}+s+b+\mathbf{A}\right|-\ln\left|s+b+\mathbf{B}\right|\right]$$

$$\mathbf{2}=\frac{k}{2\pi^3}(s+b)\ln\left|\frac{s+b+\mathbf{B}}{\frac{2\pi}{k}+s+b+\mathbf{A}}\right|$$

Solve for $\mathbf{I}$ by combining $(\mathbf{1}+\mathbf{2})$.

$$\mathbf{I} = \frac{k}{2\pi^3}\left[\mathbf{A}-\mathbf{B}+(s+b)\ln\left|\frac{s+b+\mathbf{B}}{\frac{2\pi}{k}+s+b+\mathbf{A}}\right|\right]$$

Begin solving **II** by calling the left integral **3**, middle integral **4**, and right integral **5**. Solve **3** using Eqn. (4.30).

$$-\frac{k^2}{4\pi^4}\int_{s+b}^{\frac{2\pi}{k}+s+b}\frac{\xi^2}{\sqrt{\xi^2-b^2}}\,d\xi = -\frac{k^2}{4\pi^4}\left[\frac{\xi}{2}\sqrt{\xi^2-b^2}+\frac{b^2}{2}\ln|\xi+\sqrt{\xi^2-b^2}|\right]_{s+b}^{\frac{2\pi}{k}+s+b}$$

$$= -\frac{k^2}{4\pi^4}\left[\left(\frac{\frac{2\pi}{k}+s+b}{2}\right)\mathbf{A}+\frac{b^2}{2}\ln\left|\frac{2\pi}{k}+s+b+\mathbf{A}\right|-\left(\left(\frac{s+b}{2}\mathbf{B}\right)+\frac{b^2}{2}\ln|s+b+\mathbf{B}|\right)\right]$$

$$\mathbf{3} = \frac{k^2}{4\pi^4}\left[\left(\frac{s+b}{2}\right)\mathbf{B}-\left(\frac{\frac{2\pi}{k}+s+b}{2}\right)\mathbf{A}+\frac{b^2}{2}\ln\left|\frac{s+b+\mathbf{B}}{\frac{2\pi}{k}+s+b+\mathbf{A}}\right|\right]$$

Solve **4** using Eqn. (4.28):

$$\frac{k^2}{4\pi^4}\int_{s+b}^{\frac{2\pi}{k}+s+b}2(s+b)\frac{\xi}{\sqrt{\xi^2-b^2}}\,d\xi = \frac{k^2}{4\pi^4}2(s+b)[\sqrt{\xi^2-b^2}]_{s+b}^{\frac{2\pi}{k}+s+b}$$

$$\mathbf{4} = \frac{k^2}{4\pi^4}[2(s+b)(\mathbf{A}-\mathbf{B})]$$

Solve **5** using Eqn. (4.29):

$$-\frac{k^2}{4\pi^4}\int_{s+b}^{\frac{2\pi}{k}+s+b}(s^2+2sb+b^2)\frac{1}{\sqrt{\xi^2-b^2}}\,d\xi = -\frac{k^2}{4\pi^4}(s^2+2sb+b^2)[\ln|\xi+\sqrt{\xi^2-b^2}|]_{s+b}^{\frac{2\pi}{k}+s+b}$$

$$= -\frac{k^2}{4\pi^4}(s^2+2sb+b^2)\left[\ln\left|\frac{2\pi}{k}+s+b+\mathbf{A}\right|-\ln|s+b+\mathbf{B}|\right]$$

$$\mathbf{5} = \frac{k^2}{4\pi^4}\left[(s^2+2sb+b^2)\ln\left|\frac{s+b+\mathbf{B}}{\frac{2\pi}{k}+s+b+\mathbf{A}}\right|\right]$$

Solve for **II** by combining $(\mathbf{3}+\mathbf{4}+\mathbf{5})$:

$$\mathbf{II} = \frac{k^2}{4\pi^4}\left[\left(\frac{s+b}{2}\right)\mathbf{B} - \left(\frac{\frac{2\pi}{k}+s+b}{2}\right)\mathbf{A} + \frac{b^2}{2}\ln\left|\frac{s+b+\mathbf{B}}{\frac{2\pi}{k}+s+b+\mathbf{A}}\right| \dots\right] \left[\dots + 2(s+b)(\mathbf{A}-\mathbf{B}) + (s^2+2sb+b^2)\ln\left|\frac{s+b+\mathbf{B}}{\frac{2\pi}{k}+s+b+\mathbf{A}}\right|\right]$$

Solve for the expression for λ_0 by combining $(\mathbf{I}+\mathbf{II})$:

$$\lambda_0 = \frac{k}{2\pi^3}\left[\mathbf{A}-\mathbf{B}+(s+b)\ln\left|\frac{s+b+\mathbf{B}}{\frac{2\pi}{k}+s+b+\mathbf{A}}\right|\right]\dots + \frac{k^2}{4\pi^4}\left[\frac{(s+b)\mathbf{B}}{2} - \frac{(\frac{2\pi}{k}+s+b)\mathbf{A}}{2} + \frac{b^2}{2}\ln\left|\frac{s+b+\mathbf{B}}{\frac{2\pi}{k}+s+b+A}\right| + 2(s+b)(\mathbf{A}-\mathbf{B})\dots\right] \left[\dots + (s^2+b^2+2sb)\ln\left|\frac{s+b+\mathbf{B}}{\frac{2\pi}{k}+s+b+\mathbf{A}}\right|\right]$$

Where $\mathbf{A}$ and $\mathbf{B}$ are:

$$\mathbf{A} = \sqrt{\frac{4\pi^2}{k^2}+s^2+2sb+\frac{4\pi}{k}(s+b)}$$
$$\mathbf{B} = \sqrt{s^2+2sb}$$

Multiplying by a factor of 2π as described in Section 4.4.4 gives a final answer of:

$$\lambda_0 = \frac{k}{\pi^2}\left[\mathbf{A}-\mathbf{B}+(s+b)\ln\left|\frac{s+b+\mathbf{B}}{\frac{2\pi}{k}+s+b+\mathbf{A}}\right|\right]\dots + \frac{k^2}{2\pi^3}\left[\frac{(s+b)\mathbf{B}}{2} - \frac{(\frac{2\pi}{k}+s+b)\mathbf{A}}{2} + \frac{b^2}{2}\ln\left|\frac{s+b+\mathbf{B}}{\frac{2\pi}{k}+s+b+A}\right| + 2(s+b)(\mathbf{A}-\mathbf{B})\dots\right] \left[\dots + (s^2+b^2+2sb)\ln\left|\frac{s+b+\mathbf{B}}{\frac{2\pi}{k}+s+b+\mathbf{A}}\right|\right]$$

The definitions of $\mathbf{A}$ and $\mathbf{B}$ remain unchanged.

Complete Derivation of Gamma-On λ_0 in ξ Regime

Begin with Eqn. (4.24).

$$\lambda_0 = \frac{1}{2\pi} \int_b^\infty \frac{\gamma_w}{\sqrt{\xi^2 - b^2}}\, d\xi$$

Substitute in Γ^* from Eqn. (4.3) for γ_w. Alter the integration bounds such that they match those determined for the Gamma-On condition in Section 4.4.2.

$$\lambda_0 = \frac{1}{2\pi} \int_b^{\frac{2\pi}{k}-\Delta+b} \frac{\frac{k}{\pi^2}T - \frac{k^2}{2\pi^3}T^2}{\sqrt{\xi^2 - b^2}}\, d\xi$$

Substitute $T = \xi + \Delta - b$ also from the Gamma-On portion of Section 4.4.2.

$$\lambda_0 = \frac{1}{2\pi} \int_b^{\frac{2\pi}{k}-\Delta+b} \frac{\frac{k}{\pi^2}(\xi + \Delta - b) - \frac{k^2}{2\pi^3}(\xi + \Delta - b)^2}{\sqrt{\xi^2 - b^2}}\, d\xi$$

Expand into two integrals:

$$\lambda_0 = \frac{k}{2\pi^3} \int_b^{\frac{2\pi}{k}-\Delta+b} \frac{(\xi + \Delta - b)}{\sqrt{\xi^2 - b^2}}\, d\xi \ldots$$
$$- \frac{k^2}{4\pi^4} \int_b^{\frac{2\pi}{k}-\Delta+b} \frac{(\xi^2 + 2\xi(\Delta - b) + (\Delta^2 - 2\Delta b + b^2))}{\sqrt{\xi^2 - b^2}}\, d\xi$$

Expand left integral and call it **I**, doing the same to the right integral and calling it **II**.

$$\mathbf{I} = \frac{k}{2\pi^3} \int_b^{\frac{2\pi}{k}-\Delta+b} \left[\frac{\xi}{\sqrt{\xi^2 - b^2}} + \frac{(\Delta - b)}{\sqrt{\xi^2 - b^2}} \right] d\xi$$

$$\mathbf{II} = -\frac{k^2}{4\pi^4} \int_b^{\frac{2\pi}{k}-\Delta+b} \left[\frac{\xi^2}{\sqrt{\xi^2 - b^2}} + \frac{2(\Delta - b)\xi}{\sqrt{\xi^2 - b^2}} + \frac{(\Delta^2 - 2\Delta b + b^2)}{\sqrt{\xi^2 - b^2}} \right] d\xi$$

Begin with **I**. Call left integral **1** and right integral **2**. Integrating **1** using Eqn. (4.28) results in:

$$\frac{k}{2\pi^3}\int_b^{\frac{2\pi}{k}-\Delta+b}\frac{\xi}{\sqrt{\xi^2-b^2}}\,d\xi=\frac{k}{2\pi^3}[\sqrt{\xi^2-b^2}]_b^{\frac{2\pi}{k}-\Delta+b}$$

$$=\frac{k}{2\pi^3}\left[\sqrt{\left(\frac{2\pi}{k}-\Delta+b\right)^2-b^2}-\sqrt{b^2-b^2}\right]$$

$$=\frac{k}{2\pi^3}\left[\sqrt{\frac{4\pi^2}{k^2}+\frac{4\pi}{k}(b-\Delta)+\Delta^2-2\Delta b}\right]$$

$$\mathbf{1}=\frac{k}{2\pi^3}\mathbf{C}$$

Where **C** is defined as:

$$\mathbf{C}=\sqrt{\frac{4\pi^2}{k^2}+\frac{4\pi}{k}(b-\Delta)+\Delta^2-2\Delta b}$$

Move to integral **2** and integrate with Eqn. (4.29).

$$\frac{k}{2\pi^3}\int_b^{\frac{2\pi}{k}-\Delta+b}\frac{(\Delta-b)}{\sqrt{\xi^2-b^2}}\,d\xi=\frac{k}{2\pi^3}\left[(\Delta-b)\ln\left|\xi+\sqrt{\xi^2-b^2}\right|\right]_b^{\frac{2\pi}{k}-\Delta+b}$$

$$=\frac{k}{2\pi^3}(\Delta-b)\left[\ln\left|\frac{2\pi}{k}-\Delta+b+\sqrt{\left(\frac{2\pi}{k}-\Delta+b\right)^2-b^2}\right|-\ln|b+\sqrt{b^2-b^2}|\right]$$

$$=\frac{k}{2\pi^3}(\Delta-b)\left[\ln\left|\frac{2\pi}{k}-\Delta+b+\mathbf{C}\right|-\ln|b|\right]$$

$$\mathbf{2}=\frac{k}{2\pi^3}(\Delta-b)\ln\left|\frac{\frac{2\pi}{k}-\Delta+b+\mathbf{C}}{b}\right|$$

Solve for **I** by combining $(\mathbf{1}+\mathbf{2})$.

$$\mathbf{I}=\frac{k}{2\pi^3}\left[\mathbf{C}+(\Delta-b)\ln\left|\frac{\frac{2\pi}{k}-\Delta+b+\mathbf{C}}{b}\right|\right]$$

Begin solving **II** by calling the left integral **3**, middle integral **4**, and right integral **5**. Solve **3** using Eqn. (4.30).

$$-\frac{k^2}{4\pi^4}\int_b^{\frac{2\pi}{k}-\Delta+b}\frac{\xi^2}{\sqrt{\xi^2-b^2}}\,d\xi = -\frac{k^2}{4\pi^4}\left[\frac{\xi}{2}\sqrt{\xi^2-b^2}+\frac{b^2}{2}\ln|\xi+\sqrt{\xi^2-b^2}|\right]_b^{\frac{2\pi}{k}-\Delta+b}$$

$$= -\frac{k^2}{4\pi^4}\left[\left(\frac{\frac{2\pi}{k}-\Delta+b}{2}\right)\mathbf{C}+\frac{b^2}{2}\ln\left|\frac{2\pi}{k}-\Delta+b+\mathbf{C}\right|-\left(\frac{b^2}{2}\ln|b|\right)\right]$$

$$\mathbf{3} = \frac{k^2}{4\pi^4}\left[\frac{b^2}{2}\ln\left|\frac{b}{\frac{2\pi}{k}-\Delta+b+\mathbf{C}}\right|-\left(\frac{\frac{2\pi}{k}-\Delta+b}{2}\right)\mathbf{C}\right]$$

Solve **4** using Eqn. (4.28):

$$-\frac{k^2}{4\pi^4}\int_b^{\frac{2\pi}{k}-\Delta+b}2(\Delta-b)\frac{\xi}{\sqrt{\xi^2-b^2}}\,d\xi = \frac{k^2}{4\pi^4}2(\Delta-b)[\sqrt{\xi^2-b^2}]_b^{\frac{2\pi}{k}-\Delta+b}$$

$$\mathbf{4} = \frac{k^2}{4\pi^4}[-2(\Delta-b)\mathbf{C}]$$

Solve **5** using Eqn. (4.29):

$$-\frac{k^2}{4\pi^4}\int_b^{\frac{2\pi}{k}-\Delta+b}(\Delta^2-2\Delta b+b^2)\frac{1}{\sqrt{\xi^2-b^2}}\,d\xi = -\frac{k^2}{4\pi^4}(\Delta^2-2\Delta b+b^2)[\ln|\xi+\sqrt{\xi^2-b^2}|]_b^{\frac{2\pi}{k}-\Delta+b}$$

$$= -\frac{k^2}{4\pi^4}(\Delta^2-2\Delta b+b^2)\left[\ln\left|\frac{2\pi}{k}-\Delta+b+\mathbf{C}\right|-\ln|b|\right]$$

$$\mathbf{5} = \frac{k^2}{4\pi^4}\left[(\Delta^2-2\Delta b+b^2)\ln\left|\frac{b}{\frac{2\pi}{k}-\Delta+b+\mathbf{C}}\right|\right]$$

Solve for **II** by combining $(\mathbf{3}+\mathbf{4}+\mathbf{5})$:

$$\mathbf{II} = \frac{k^2}{4\pi^4}\left[\frac{b^2}{2}\ln\left|\frac{b}{\frac{2\pi}{k}-\Delta+b+\mathbf{C}}\right|-\left(\frac{\frac{2\pi}{k}-\Delta+b}{2}\right)\mathbf{C}\ldots\right]$$
$$\left[\cdots-2(\Delta-b)\mathbf{C}+(\Delta^2-2\Delta b+b^2)\ln\left|\frac{b}{\frac{2\pi}{k}-\Delta+b+\mathbf{C}}\right|\right]$$

Solve for the expression for λ_0 by combining $(\mathbf{I} + \mathbf{II})$:

$$\lambda_0 = \frac{k}{2\pi^3}\left[\mathbf{C} + (\Delta - b)\ln\left|\frac{\frac{2\pi}{k} - \Delta + b + \mathbf{C}}{b}\right|\right]\dots$$
$$+ \frac{k^2}{4\pi^4}\left[\frac{b^2}{2}\ln\left|\frac{b}{\frac{2\pi}{k} - \Delta + b + \mathbf{C}}\right| - \frac{(\frac{2\pi}{k} - \Delta + b)\mathbf{C}}{2} - 2(\Delta - b)\mathbf{C}\dots\right]$$
$$\left[\dots + (\Delta^2 - 2\Delta b + b^2)\ln\left|\frac{b}{\frac{2\pi}{k} - \Delta + b + \mathbf{C}}\right|\right]$$

Where $\mathbf{C}$ is defined by:

$$\mathbf{C} = \sqrt{\frac{4\pi^2}{k^2} + \frac{4\pi}{k}(b - \Delta) + \Delta^2 - 2\Delta b}$$

Multiplying by a factor of 2π as described in Section 4.4.4 gives a final answer of:

$$\lambda_0 = \frac{k}{\pi^2}\left[\mathbf{C} + (\Delta - b)\ln\left|\frac{\frac{2\pi}{k} - \Delta + b + \mathbf{C}}{b}\right|\right]\dots$$
$$+ \frac{k^2}{2\pi^3}\left[\frac{b^2}{2}\ln\left|\frac{b}{\frac{2\pi}{k} - \Delta + b + \mathbf{C}}\right| - \frac{(\frac{2\pi}{k} - \Delta + b)\mathbf{C}}{2} - 2(\Delta - b)\mathbf{C}\dots\right]$$
$$\left[\dots + (\Delta^2 - 2\Delta b + b^2)\ln\left|\frac{b}{\frac{2\pi}{k} - \Delta + b + \mathbf{C}}\right|\right]$$

The definition of $\mathbf{C}$ remains unchanged.

Figures

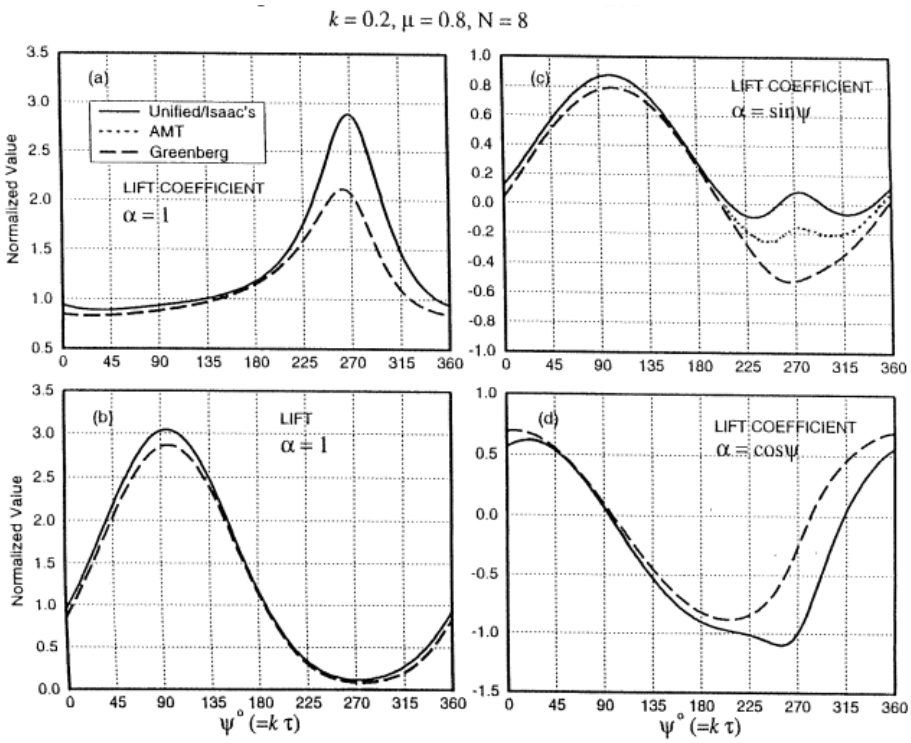

Figure 1: Peters-Barwey Paper's Results for Airloads in a Periodic Freestream (Taken Directly from Ref. [2])

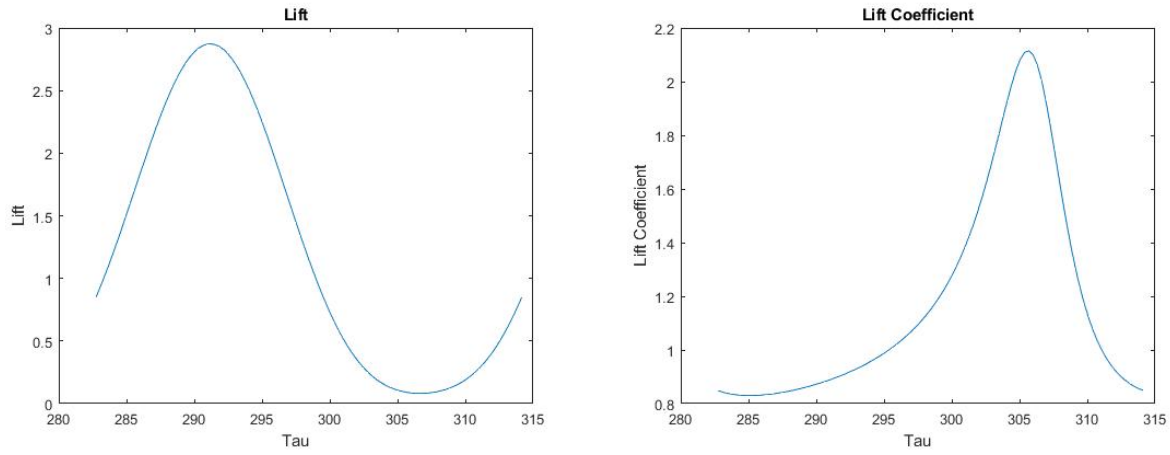

Figure 2: Greenberg Lift and Lift Coefficient of $\alpha = 1$

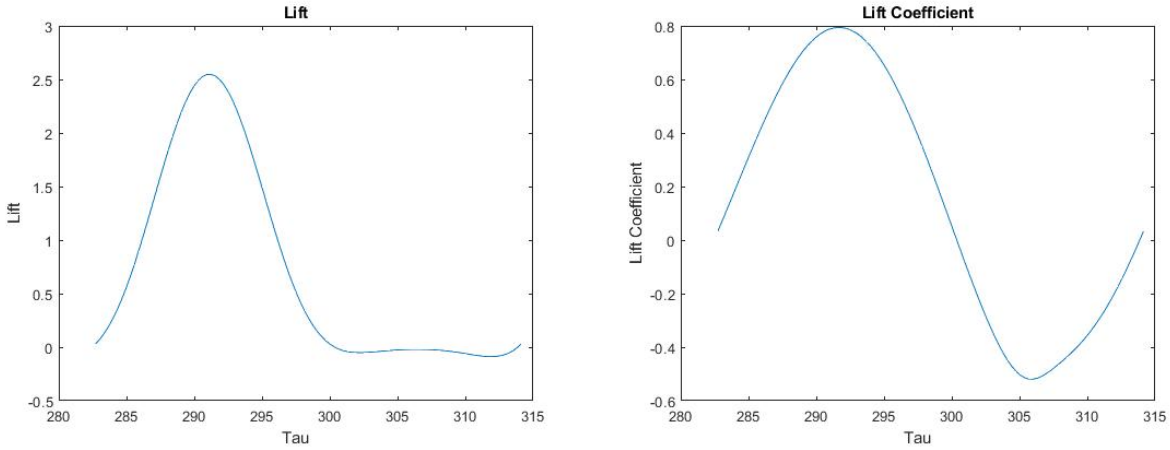

Figure 3: Greenberg Lift and Lift Coefficient of $\alpha = sin(k\tau)$

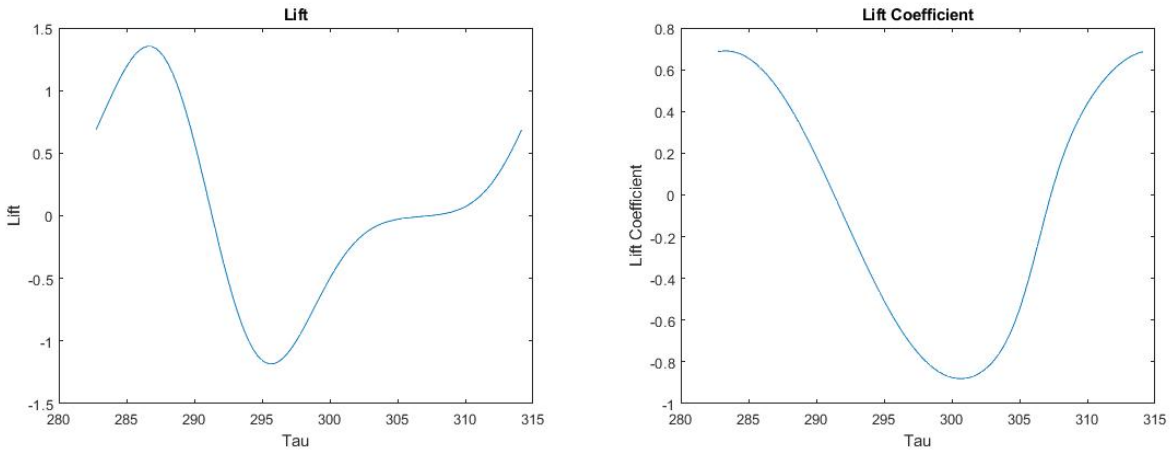

Figure 4: Greenberg Lift and Lift Coefficient of $\alpha = cos(k\tau)$

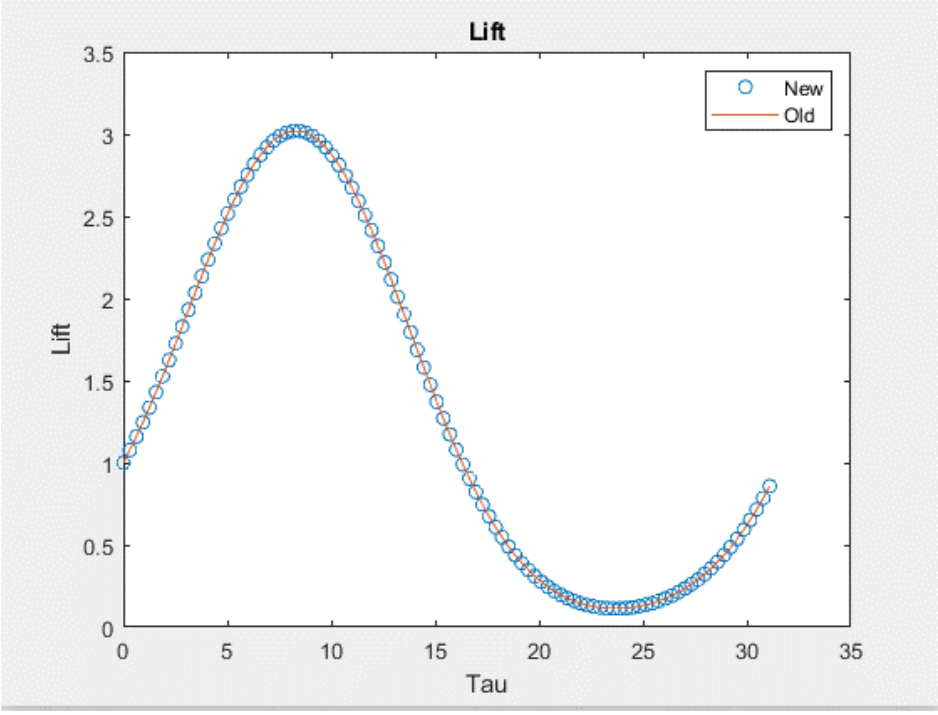

Figure 5: Robust Test Case with $\alpha = 1, u_0 = 1 + \mu sin(k\tau)$

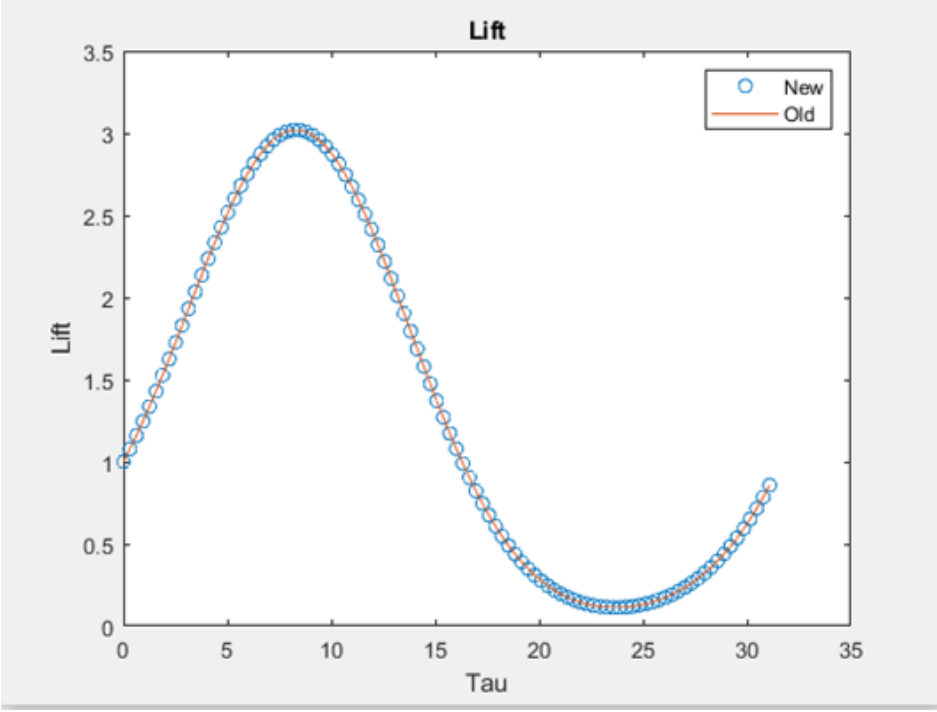

Figure 6: Robust Test Case with $\alpha = -1, u_0 = -1 - \mu sin(k\tau)$

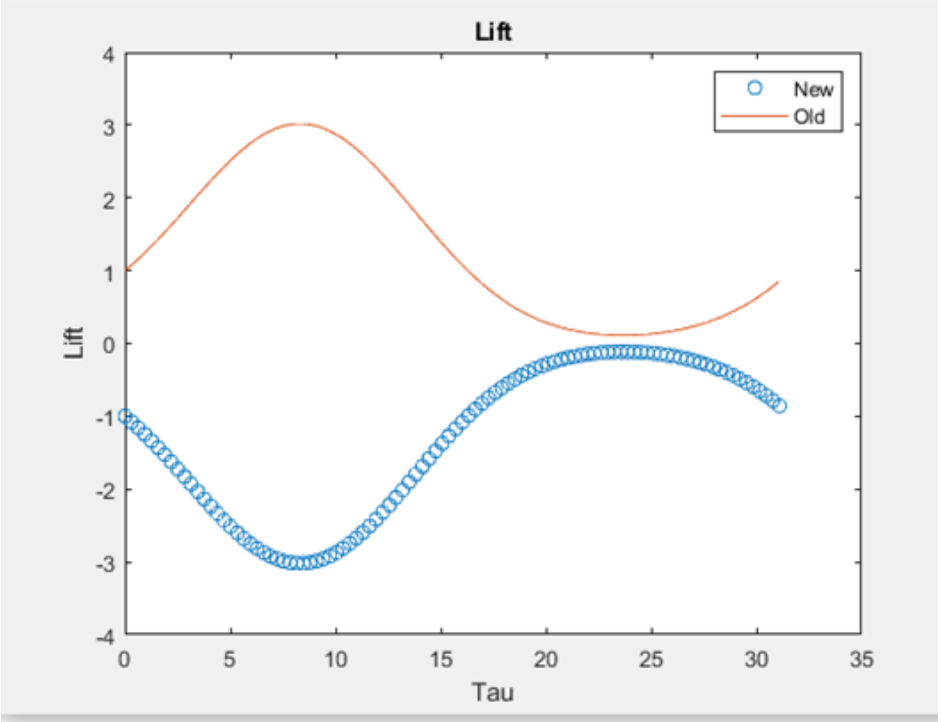

Figure 7: Robust Test Case with $\alpha = 1, u_0 = -1 - \mu sin(k\tau)$

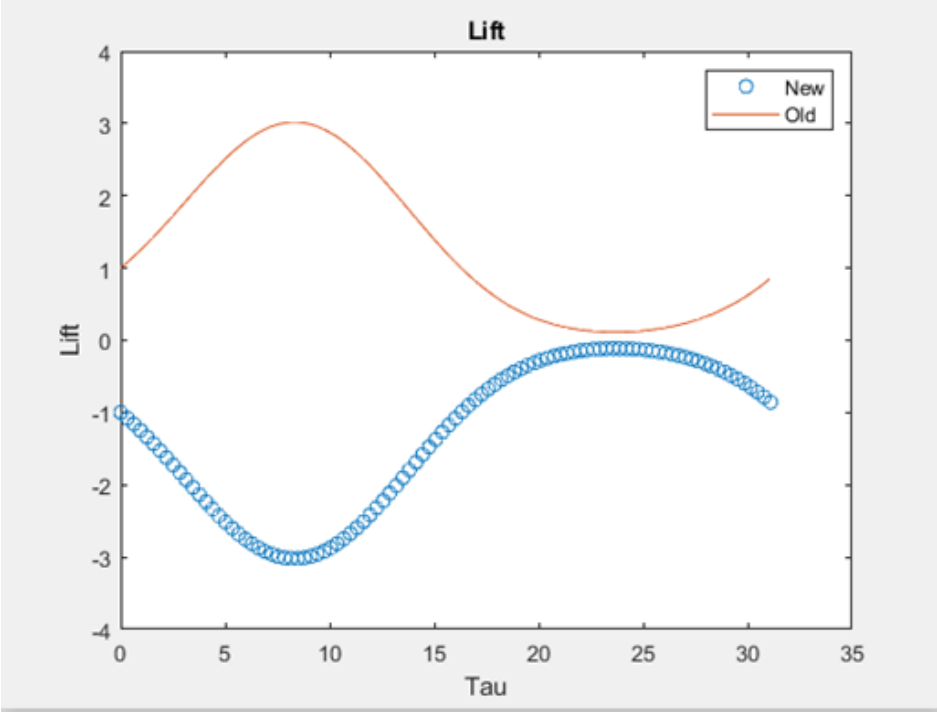

Figure 8: Robust Test Case with $\alpha = -1, u_0 = 1 + \mu sin(k\tau)$